AALBORG UNIVERSITET

Faculty of Engineering, Science, and Medicine
Aalborg University

Department of Biotechnology, Chemistry, and Environmental Engineering.
Section of Chemistry

TITLE:
Modification of Metal Surfaces Using a Polystyrene Template

- Electric Potential Controlled Particle Deposition

MASTER THESIS
September 1st 2007 -
May 31th 2008

PROJECT AUTHOR:
Jeanette Rosa Pedersen

SUPERVISOR:
Mogens Hinge

NUMBER OF COPIES: 4

REPORT PAGES: 63

APPENDIX PAGES: 8

ENCLOSURE PAGES: 1

TOTAL PAGES: 73

ENCLOSED: CD-rom

Abstract:

It was attempted to modify Cu, Al, and Cr surfaces by the use of a polystyrene template. The aim of the modification was a rough surface with a high water contact angle (CA). It was attempted to create the polystyrene (PS) template by a combination of a thin liquid film deposition (TLFD) technique and an electric potential. The TLFD technique was applied to utilize lateral capillary forces. The electric potential was applied because it, in literature, had been observed to enhance the lateral capillary forces. It was desired to achieve a template of closed-packed (CP) particles in mono-layer with a hexagonal lattice on the metal surfaces, to obtain the smallest solid fraction possible. Scanning electron microscopy and contact angle measurements were used to analyse the samples. Furthermore, dynamic light scattering was used to analyse the particles.
The characterization of the metal surfaces showed large crystals on the Al surface. Therefore, Al was not used for further experiments. Cr had a porous surface and a CA of $95 \pm 12°$. Cu had a planar surface and a CA of $84 \pm 7°$.
From experiments using the TLFD technique and glass slides, a PS concentration of 24 g/L and the withdrawal rates of $3 \cdot 10^{-2}$ and $1 \cdot 10^{-1}$ mm/s were found to be optimal for further investigations.
The metal surfaces responded differently to the TLFD technique than the glass slides. This seemed to be caused by different surface structures and wettabilities of the surfaces.
With the TLFD technique multi-layers were formed on the metal surfaces. Therefore, a positively charged potential was applied on the surface. Cr was not conductive, thus, the effect of the potential could only be considered from the Cu samples. The potential resulted in particles being repelled from the surface, and a thinner film was achieved. The effect was distinct when applying a potential of 300 mV. CP particle mono-layer with a hexagonal lattice were observed in some areas of the surfaces.
It was attempted to remove the particles from gold coated samples. Heating of the sample for 2 hours at 550°C resulted in crystals of several micrometers on the surface. Furthermore, the particles seemed to have shrunk, but had not been removed. The particles had also not been removed by the wash with toluene for 43 hours, but the sonication of samples in toluene for 5 minutes seemed to be the most effective method.

AALBORG UNIVERSITET

Det ingeniør-, natur-, og sunhedsvidenskabelige fakultet
Aalborg Universitet

Institut for bioteknologi, kemi og miljøteknik.
Sektionen for kemi

TITEL:
Modifikation af metaloverflader ved brug af en polystyren skabelon

- Elektrisk potentiale kontrolleret partikel aflejring

SPECIALE
1. september 2007 -
31. maj 2008

PROJEKTFORFATTER:
Jeanette Rosa Pedersen

VEJLEDER:
Mogens Hinge

ANTAL KOPIER: 4

RAPPORT SIDEANTAL: 63

APPENDIKS SIDEANTAL: 8

BILAG SIDEANTAL: 1

TOTAL SIDEANTAL: 73

VEDLAGT: CD-rom

Synopsis:

Det blev forsøgt at modificere Cu, Al og Cr overflader ved brug af en polystyren (PS) skabelon. Målet var, at opnå en ru overflade med en stor kontaktvinkel (CA) med vand. PS skabelonen var forsøgt dannet ved en kombination af en thin liquid film deposition (TLFD) teknik og et elektrisk potentiale. TLFD teknikken blev anvendt for at udnytte lateral kapillære krafter. Det elektriske potentiale blev påført, fordi det i litteraturen blev observeret, at det kunne forstærke de lateral kapillære krafter. Det var ønsket at opnå en skabelon af tæt-pakkede (CP) partikler i et monolag med et hexagonalt mønster på metaloverfladerne. Scanning elektron mikroskopi og kontakt vinkel målinger blev brugt til analyse af prøverne.
Karakteriseringen af metaloverfladerne viste store krystaller på Al overfladen. Derfor blev Al ikke brugt til nogen videre forsøg. Cr havde en porøs overflade og en CA på $95 \pm 12°$. Cu havde en plan overflade og en CA på $84 \pm 7°$.
Udfra forsøg med TLFD teknikken og glasoverflader blev en PS koncentration på 24 g/L og trækhastighederne på $3 \cdot 10^{-2}$ og $1 \cdot 10^{-1}$ mm/s fundet til at være optimale.
Metaloverfladerne reagerede anderledes på TLFD teknikken end glasoverfladerne. Dette syntes at skyldes, at overfladerne havde forskellige overflade-strukturer og spændinger.
Med TLFD teknikken blev der dannet multilag på metaloverfladerne, og derfor blev der tilført et positivt potentiale til overfladerne. Cr ledte ikke strømmen, og derfor kunne effekten af potentialet kun vurderes ud fra Cu prøverne. Potentialet resulterede i at partikler blev frastødt, og en tyndere film blev opnået. Effekten var tydeligst ved et potentiale på 300 mV. CP partikelmonolag med et hexagonalt mønster blev observeret i nogle områder på nogle af prøverne.
Det blev forsøgt at fjerne partiklerne fra guldbelagte prøver. Opvarmning til 550°C i 2 timer resulterede i dannelse af krystaller på overfladen. Desuden syntes partiklerne at have skrumpet, men var ikke fjernet. Partiklerne blev heller ikke fjernet ved vask med toluen i 43 timer, men påvirkningen af ultralyd i toluen syntes at være mest effektiv.

Preface

This report is a master thesis prepared at 9.-10. semester at the section of chemistry, Department of Biotechnology, Chemistry, and Environmental Engineering at Aalborg Universtity.

All references in the report are stated in accordance with the Harvard method and is listed alphabetically according to writer's surname in the end of the report.

The project is divided into chapters that are consecutive numbered. Figures, tables, and equations are numbered similar to the chapter, but the first number is a reference to the given chapter.

A CD-ROM containing all data from the different analyses is enclosed. The notation "Enclosure CD - name of the folder" is used when referring to the CD. Additionally, experimental treatments, the referred articles, and a copy of the report (pdf) can be found on the CD.

I would like to express thanks to Jens Rafaelsen, Department of Physics and Nanotechnology, Aalborg University, for introducing and helping with the scanning electron microscopy. Furthermore, I would like to acknowledge Teknologisk Institut, Århus, for contributing with the metal pre-coated slides in the project.

.....

Jeanette Rosa Pedersen

Contents

Chapter 1

Introduction

Super-hydrophobic (SH) surfaces are of special interest because of anti-sticking, anti-contamination, and self-cleaning properties etc. The properties of the SH surfaces could have industrial and biological applications such as anti-biofouling paints for boats, anti-sticking of snow for antennas and windows, self-cleaning windshields for automobiles etc. [Li *et al.*, 2007]. A SH surface is characterized as a surface with a contact angle (CA) higher than 150° [Li *et al.*, 2007]. Many examples of SH surfaces are seen in nature, such as water strider legs, butterfly wings, duck feathers, and the leaves of the lotus flower [Quere, 2005]. The leaves of the lotus flower have a two-scale roughness, one around 10 μm and one around 100 nm, shown in Figure 1.1 [Li *et al.*, 2007].

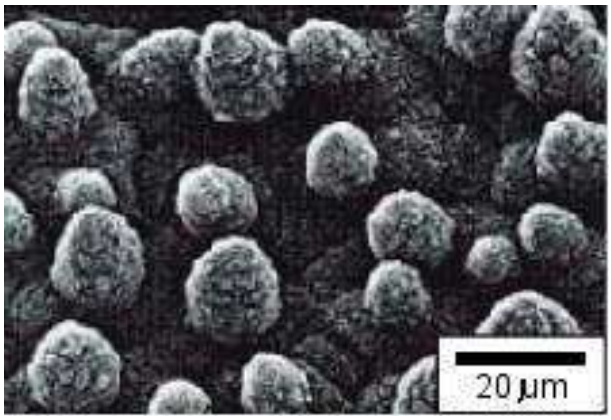

Figure 1.1: A SEM image of the lotus leave showing the two-scale roughness [Baumann *et al.*, 2003].

Furthermore, the leaves of the flower secrete epicuticular wax, containing predominantly -CH_2- groups, and hereby the wax possesses a water CA of about 110° [Ma and Hill, 2006; Li *et al.*, 2007]. Altogether, the micro- and nanoscale structures and the low surface energy of the wax contribute to a water CA of 161± 2.7° and a CA hysteresis of 2° [Li *et al.*, 2007]. The CA hysteresis gives information on the solid-liquid interaction. If the hysteresis is low, the drop is in the Cassie-Baxter ("slippy") state, and a high hysteresis denotes the Wenzel ("sticky") state [Martines *et al.*, 2005]. Thus, the low hysteresis of the water CA on the lotus leaf causes the water droplets to roll of the leaves while collecting contaminants. A self-cleaning effect,

called the "Lotus effect" [Li *et al.*, 2007]. The two-scale roughness of the lotus leaf has been proven to enhance the water repellency. Additionally, the roughness of materials at small scale (nanometric) alone has been suggested to play an important role on water repellency. Thus, the nanometric structures on wings of some insects are thought to ensure the water repellency [Martines *et al.*, 2005].

There are several ways in which a SH surface can be obtained. Examples of preparation could be by use of aligned carbon nanotube (ACNT) films, where the nanotubes are perpendicular to the substrate, creating a rough surface structure [Li *et al.*, 2001]. Furthermore, porous microsphere/nanofiber composite films have been prepared. Here microparticles were covered with nanopapilla, creating lotus-leaf-like structures [Jiang *et al.*, 2004]. SH surfaces have also been obtained from nanopillar arrays made through "template rolling press" of polycarbonate [Guo *et al.*, 2004], and further nanoimprinting and wet-chemical etching on silicon have also been used to create nanopillars, and hereby a rough surface that possessed SH properties [Pozzato *et al.*, 2006]. SH metal surfaces have been prepared by utilization of dislocation-selective etching that make pillars on the surface by attacking crystal defects. Afterward the surface was coated with a low surface tension material that provided the SH properties [Qian and Shen, 2005]. In general, when manufacturing SH surfaces, both chemical composition and geometrical micro- or nanostructures of the surface are crucial parameters that determines the hydrophobicity [Yang *et al.*, 2006]. Thus, this was also observed when studying the leaves of the lotus flower. Therefore, SH surfaces can be achieved either by making a material with low surface energy rough, or by making a rough surface and afterward modifying the surface with a low surface energy material [Ma and Hill, 2006].

Many of the methods used for preparation of SH surfaces are in small scale and are difficult to use in larger scale. But it could be a possibility to use the property of particle self-assembly on materials in larger scale [Hanarp *et al.*, 2003]. Polystyrene (PS) particles have previously been used as templates for modification of surfaces [Abdelsalam *et al.*, 2005] and their ability to self-organize (where CP particles with a hexagonal lattice is the most favorable pattern [Nagayama, 1996]) can be used to form ordered structures. The parallel nature of the assembly process makes it possible to produce large numbers of nanosized features and/or to cover large areas of materials [Hanarp *et al.*, 2003]. Therefore, it is interesting to investigate the possibilities of controlling or enhancing the self-assembly technique.

Chapter 2

Background Theory

Many investigations have been done on assembling of particles onto surfaces, and many different methods have been applied. This chapter summarises some of the previous works.

Structuring of Gold Surfaces by a Template

Abdelsalam and coworkers (2005) have reported a study of the wetting of regularly structured gold surfaces. The surface was obtained by using gold electrodes as substrates and 500 nm PS spheres in a mono-layer as template. The PS particles were deposited in a thin layer cell (2 cm $\times$ 1.5 cm) made of a gold electrodes deposited with cysteamine and a clean uncoated microscope coverglass. The gold electrode and the coverglass were held 100 μm apart by parafilm, and the space between the two plates was filled with an aqueous 1wt% (10 g/L) suspension of PS spheres. The cell was held vertically in an incubator to control the rate of evaporation from the cell. When dry the templates were robust, adhered to the gold substrate and were opalescent. Gold was then electrochemically deposited on the template-coated gold substrate. After the deposition of gold, the spheres were removed from the substrate by dissolving the PS spheres in tetrahydrofuran and left was a porous metal film with regular cavities filled with air, as seen in Figure 2.1.

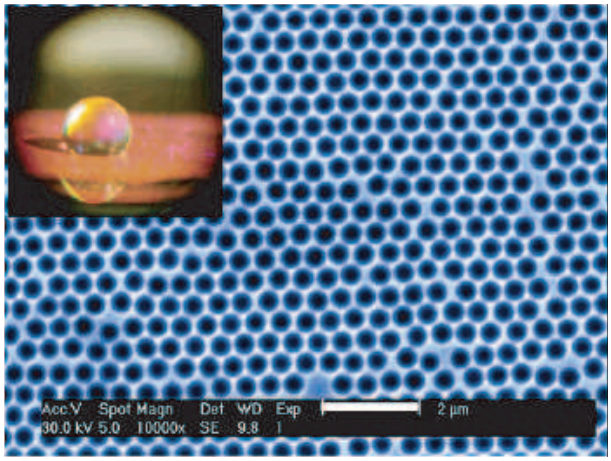

Figure 2.1: SEM image of an electrochemically deposited gold film, created by using a PS template with 500-nm-diameter spheres. The image in the left corner shows a 5 μL drop of water placed on the film. The apparent CA (θ^*) is $\theta^* = 131°$ [Abdelsalam *et al.*, 2005].

A highly ordered pore structure was obtained in the film. The pore diameter was directly determined by the diameter of the PS spheres used to form the template. An untreated gold surface possesses a CA of 70°, but the hexagonal array of air-filled pores in the gold film gave a rough film, which made the otherwise hydrophilic surface hydrophobic with a CA of 131°. The mouths of the pores were nearly circular at all thicknesses. It was observed that the film wettability changed with the changes in the solid fraction. Hereby, changes in the fraction of solid interacting with liquid. Film thicknesses up to half the template sphere diameter $\xi < 1/2$ (ξ: the film thickness divided by the pore diameter) had an increasing CA, in correlation to an increasing mouth diameter and hereby an increasing surface void fraction of the area underneath the water drop. For film thicknesses from half a sphere diameter up to one sphere diameter ($1/2 < \xi < 1$), the CA decreased, which is caused by the mouth of the pores decreasing in diameter. Hereby, larger interactions between the solid fraction of the surface and the water droplet occur [Abdelsalam *et al.*, 2005].

Furthermore, the water CA was measured on film made with different templates of different sphere diameters (400-800 nm). It was concluded, when having a constant film thickness (ξ of approximately 0.12), that the pore size had no significant influence on the CA in the range from 400-800 nm, although the center-to-center separation of the cavities changed [Abdelsalam *et al.*, 2005].

Control of Nanoparticle Film Structure

Hanarp and coworkers (2003) have investigated the possibility of controlling the nanoparticle film structure for colloidal lithography. It was desired to control the colloidal mono-layer films where particle size and particle coverage (measured as area of particles divided by total area) could be changed systematically. It was found that this required control of both adsorption of particles onto the substrates as well as control of the subsequent drying of the film on the substrates. In the experiments negatively charged PS spheres (diameter: 41 $\pm$ 6, 107 $\pm$ 5, 200 $\pm$ 6, and 530 $\pm$ 27 nm) in solution concentrations of 1 - 5 g/L were used to adsorb onto positively charged

flat titanium oxide substrates. The positively charged surface on titanium oxide substrates was achieved, by coating the substrate with a triple layer of poly(diallyldimethylammonium chloride) (PDDA)/ poly(sodium 4-styrenesulfonate) (PSS)/ aluminium chloride hydroxide (ACH). NaCl concentrations between 0 and 100 mM were applied to the solution of particles. Adsorption time onto the substrates was varied between 1 and 30 minutes to allow adsorption saturation. Excess particles on the substrates were removed with running water and the surfaces were dried with nitrogen gas. It was attempted to prevent particle aggregation during drying because it was desired to maintain the distances between the particles. Two methods were applied, 1) adsorption of silica particles in between the larger PS particles and 2) heat treatment of the PS particles by placing the substrate in a beaker with boiling water for 30 s directly after the deposition of particles. Furthermore, oxygen plasma treatments was used to modify the particle size.

The triple layer of PDDA/PSS/ACH on the substrate seemed to have an influence on the adsorption of particles. This layer gave an excellent quality film compared to when only PDDA or ACH were used. The particle coverage of a specific particle film was mainly controlled by the ionic strength in the solution. The higher the salt concentration, the more the electrostatic repulsion between the particles was screened, and the particles could adsorb closer together. Thus, higher salt concentration leads to higher particle coverage. For particles with a diameter of 107 nm, a low particle coverage limit of 0.12 was found with no salt added (electrolyte < 0.02 mM). Changing the particle concentrations did not seem to have any influence on the particle coverage. To obtain lower particle coverages than 0.12, oxygen plasma treatments were used. A particle coverage of 0.40 was obtained with a salt concentration of 10 mM and with 107 nm particles. For higher particle coverages, a higher ionic strength was applied. The higher ionic strength increased the particle coverage, but did also induce particle aggregation and resulted in clusters of particles with empty spaces between the clusters. A salt concentration of 40 mM resulted in 3D aggregation of the particles. Aggregation of the particle film was observed when drying the film. The solution to this problem was found from both above-mentioned methods because changes in the drying method was found to prevent the particles from aggregating, and hereby the separation between the particles was maintained. An increasing aggregation was found when using larger particles, and this indicate stronger intermolecular forces (capillary forces). The larger particles did not seem to be influenced by the heat treatments, but the absorption of silica particles between the large particles helped keeping them apart [Hanarp *et al.*, 2003].

Thin Liquid Film Depositions Technique

Dimitrov and Nagayama (1996) have used a thin liquid film deposition (TLFD) technique in an investigation of how to control the growth of particle arrays. The technique utilizes the self-assembly of particles. When a substrate is withdrawn from a liquid in a vertical direction, the particles become trapped in a thin liquid layer, and a growth of particle array starts in opposite direction of the substrate withdrawing direction. This is caused by evaporation of liquid from the substrate, which initiates particle self-assembly, when the layer thickness (h) equals the particle diameter. This is because the liquid layer is deformed when the particles is protruding their heads from the solvent surface. Hereby, a strong attraction between the particles arises. This is

also named lateral capillary forces or more specific lateral immersion forces. The deformation of the liquid surface is related to the wetting properties of the particle surface and not the gravity which would have been the case of floating particles (lateral flotation forces). The flotation and immersion forces can be both attractive and repulsive, and for two identical particles the lateral capillary force will always be attractive. The immersion forces may be one of the main reasons for the self-assembly of small colloid particles [Kralchevsky and Nagayama, 2000]. Furthermore, the evaporation of water (j_e) induced by the TLFD technique gives a flux of water (j_w) toward the substrate in the suspension, to compensate the evaporated water. This induces a flux of particles (j_p) toward the substrate, which gives an aggregation of the particles on the substrate as illustrated in Figure 2.2 [Dimitrov and Nagayama, 1996].

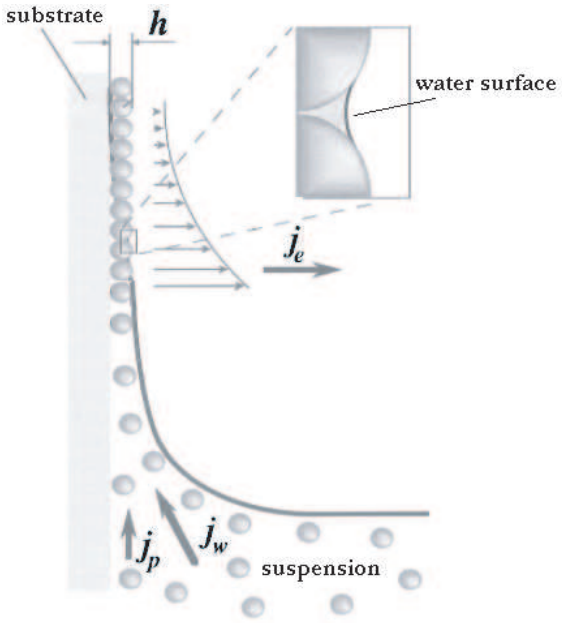

Figure 2.2: An illustration of the thin liquid film deposition (TLFD) technique. j_e is evaporation of water, j_w and j_p is the flux of water and particles toward the substrate, respectively. h is the film thickness [Dimitrov and Nagayama, 1996].

The approach of Dimitrov and Nagayama (1996) was to have a linear, continuous growth of the arrays, where the substrate was withdrawn from a suspension with a continuous rate. Furthermore, this should be the same rate as the growing arrays. Secondly, a quantitative analysis of the array growth rate was desired, and hereby it was wanted to clarify the parameters that govern the growth process. The idea was to make it possible to make large-sized homogeneous arrays, and further to control the acceleration or deceleration of the array production by changing the environmental conditions such as humidity, temperature, and particle volume fraction.

From previous experiments it was known, that when having a atmosphere relatively saturated with water vapors, the initiation of the assembling of particles was extremely slowly, whereas when having an unsaturated atmosphere the particles were assembling rather quickly. In the last-mentioned case, the rate of the assembling, caused by the evaporation of water from the film, becomes much higher than the rate of assembling, caused by lateral capillary forces. Using glass slides, coated with sodium dodecyl sulfate (SDS), as surface, polycrystalline mono-layers were achieved with the film formation technique. This was obtained using particles with diameters

ranging from approximately 80 to approximately 2100 nm. The particles and the glass slide used for this assembling was both negatively charged, and thereby an electrostatic repulsion between the surface and the particles was present, when close contact occurred. The interparticle electrostatic repulsion and the hydrodynamic water influx pressure determined the dense packing of the particles. Moreover, the close neighboring particles was attracted to each other by lateral capillary immersion forces, which did also contribute to the close-packing of particles. Special attention was given to particles with diameters larger than 400 nm, in that the centimeter-sized mono-layer particle arrays made from these particles showed opalescence. The experiments were performed at a temperature of 23.7 $\pm$ 0.5 °C and with a relative humidity of 50 $\pm$ 2%. The substrates was withdrawn with a rate from 0.1 to 30 μm/s ($1 \cdot 10^{-4}$ to $3 \cdot 10^{-2}$ mm/s) [Dimitrov and Nagayama, 1996].

The simplest way to initiate and maintain a linear growth of particle arrays was by dipping a wettable solid surface in a suspension of particles. When the surface was kept stationary, spontaneously mono- and multi-layers of particles start to grow on the surface, from the surface-suspension-air contact line down to the bulk suspension. When withdrawing the surface carefully, a homogeneous formation of mono- and multi-layer could be achieved. When the withdrawal rate equaled the growth rate, the arrays could be continuously formed to any size. The growth of particle arrays was found to start because of the water evaporation from the film. Hence, when the particles protrude their heads. The lateral capillary force can not initiate the particle array growth [Dimitrov and Nagayama, 1996].

It was concluded that the technique worked without pitfalls if no impurities was present in the suspension, the atmosphere around the experimental cell, the substrate plate, and the cell itself. Furthermore, the substrate plate should be completely wettable by the suspension, the particles should be monodispersed and should not adsorb onto the substrate. Polydispersity of the particles can create instability in the array growth. Slightly different particle sizes creates dislocations which often only influences small sizes of the domain. Impurities and particle aggregations can cause multi-layers. When the particles do not adsorb onto the surface, the particles have an ability of sliding on the surface before the film dries. Hence, the attractive coulomb forces between a positively and a negatively charged surface hinders the mobility of the particles. In case of adsorbing particles, a formation of amorphous layers is expected. Moreover, it is generally important that the suspension, from which the substrate was withdrawn, was stable. Thus, particle sinking must be prevented in case of larger particles (≈ 1 μm and above). Water vapor saturated atmosphere was essential to prevent particle aggregation at the suspension surface, and to restrict the evaporation to be mainly near the particle film. Furthermore, the evaporation from the film should be slow enough, to make sure that the array film is not ruptured or stripped [Dimitrov and Nagayama, 1996].

Electrohydrodynamic Manipulation of Particle Deposition

Trau and coworkers (1996) have reported on a method allowing layer-by-layer deposition of 2D and 3D colloidal crystals on electrode surfaces through electrohydrodynamic manipulation.

Submono-layers of PS particles were electrophoretic deposited onto an indium tin oxide (ITO) electrode. The film deposition was performed with PS particles (2 μm) from a dilute suspension,

and the particle suspension was stabilized by ionic and nonionic surfactants. When a weak electric field (≈ 0.5 V) was applied to the system or when the particles settled onto the electrode "gaseous" 2D structures was formed across the dilute suspension. The particles was not adhered to the electrode, but could freely move in two dimensions through Brownian motions. The 2D mobility of the particles was present regardless of the large electrostatic attraction between the positively charged electrode and the negatively charged particles. Thus, it seemed to be a consequence of the stabilization of the PS particles. When the voltage was increased (from 0.5 to 1.5 V) the particles moved toward one another across the electrode surface. The lateral attraction between the particles acted normal in spite of the applied field and was strong enough to bring the particles together to form stable 2D colloid crystals of particles. When raising the voltage even more they observed that the crystal formation was reversible. When the field was removed the particles were stirred by Brownian motions and again the "gaseous" phase was formed. By changing the magnitude of the current the strength of the lateral attraction (particle-particle interaction) could be controlled to give "gaseous", "liquid", and crystal 2D structures. This was also observed in experiments using nano-sized particles [Trau *et al.*, 1996].

Electrophoretically deposited particles were observed to migrate toward one another over distances larger than five particle diameters. Coalescence of particles with the same charge was observed, even though it would have been expected that electrostatic forces would hinder this aggregation of particles. But the attractive interaction seemed strong enough to overcome the electrostatic repulsion. The coalescence seemed to be a result of the electrohydrodynamic fluid flow that is an effect of the ionic current flowing through the solution. Manipulation of the "lateral attraction" between particles is possible by adjusting the field strength or the frequency [Trau *et al.*, 1996].

Knowledge gained from this chapter will be used when making the experimental design regarding the particle template.

Chapter 3

Experimental Design

It is desired to prepare SH metal surfaces, and therefore a roughening of the material must be performed. In this work, it will be investigated whether a rough surface can be achieved using a particle template in the surface modification process. The particle template will be deposited on the surface and afterwards sputter coated with a metal to create pillars of metal between the particles. Then, the particles will be removed, and the sputter coated metal will constitute the rough surface, as illustrated in Figure 3.1.

Figure 3.1: A sketch of the fundamental idea of the method utilized in this work. Particles are coated onto the surface, which creates a template. The sample is then sputter coated with metal, and the sputter coating results in pillars of metal in the hole created in the pattern of the template. Afterward the particles are removed.

It is desired to obtain a SH surface that is "slippy", and when this is the case the Cassie-Baxter (CB) model describes the apparent CA of the obtained rough surface (Details can be found in Appendix A)(Equation 3.1).

$$cos(\theta^C) = f(1 + cos(\theta)) - 1 \tag{3.1}$$

The apparent CA ($cos(\theta^C)$) is according to the CB model a sole function of the solid fraction (f) for a given θ. To achieve superhydrophobicity, the solid fraction should be as small as possible. When the solid fraction is as small as possible the highest air fraction is achieved (Appendix A). To gain as small a fraction of metal as possible on the surface, the template shall be a CP mono-layer of particles with a hexagonal lattice (illustrated in Figure 3.2), hence, the natural form of close-packing of monodisperse particles [Nagayama, 1996].

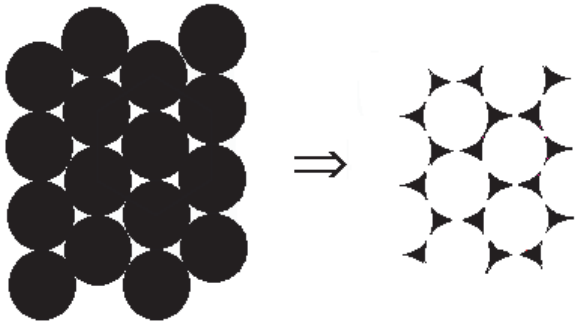

Figure 3.2: A sketch of a CP area of particles with a hexagonal lattice, and the solid fraction that is expected to be achieved if a mono-layer of particles in a hexagonal lattice is successfully used as template.

As PS particles can be obtained monodispersed and with a wide range of surface chemistries and charges, these particles could be used as a model system [Hanarp *et al.*, 2003]. The size of the PS particles can be controlled by factors as ionic strength, initiator concentration, monomer concentration, and temperature [Goodwin *et al.*, 2005]. Furthermore, the PS particles can be dissolved by organic solvents, which could become useful when the particle template shall be removed [Abdelsalam *et al.*, 2005].

The size of the particles and the coating height of the metal, that are coated between the particles, are expected to be the factors that influence the surface roughness, and hereby the SH properties of the modified surface. This is because the size of the particles and the coating height of the metal are the parameters, in this system, that influences the solid fraction, if the particles are CP in a hexagonal lattice. Therefore, the optimal particle size and the optimal coating height will be determined by a mathematical model. To estimate the optimal particle size ($r_{particle}$) and coating height (n), the solid fraction (f) will be derived as a function of these. The model can be seen in Appendix B. When deriving the solid fraction as a function of the particle size only, it was observed that no matter what particle size, the solid fraction was 0.093. Therefore, it was chosen to synthesize particles of 400 nm in average diameter, concerning all particles used in the further investigations. Hence, the particle size will be kept constant to ease the subsequent comparison of the results. Furthermore, it was from the modeling determined that the coating height should be equal to the particle radius to obtain the highest water CA of the modified surface, which was also in accordance with the observations done by Abdelsalam and coworkers (2005) (Appendix B). Additionally, according to the model it should be possible to obtain a water CA for rough surfaces obtained from chrome, aluminum, and copper, of about 153.4°,153.2°, and 156.7°, respectively.

3.1 Polystyrene Synthesis

The synthesis of the particles is chosen to be a surfactant free emulsion polymerization of styrene in water with 2,2-Azobis(2-methylpropion-amidine)dihydrochloride (V50) as initiator. The molecular structure of the initiator is seen in Figure 3.3.

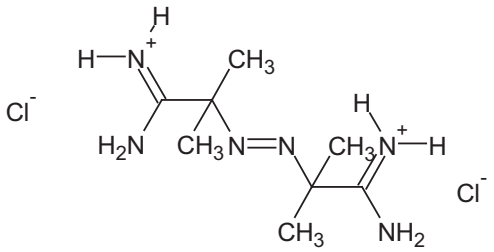

Figure 3.3: 2,2-Azobis(2-methylpropion-amidine)dihydrochloride (V50) is the initiator that will be used for the synthesis of PS particles.

When the system, containing styrene (monomer), V50, and water, is heated, the initiator starts to decompose and creating free radicals. The initiator radicals reacts with the monomer from the aqueous phase and propagates to produce oligomeric radicals which are relatively soluble in water. The oligomers, that are not terminated, grows and attain a degree of polymerization at which they become surface active. When the oligomers obtain a sufficiently degree of polymerization a micelle formation around the growing oligomer is initiated. The micelles becomes swollen with monomer and the concentration of monomer in the resulting emulsion is much higher, than in the aqueous solution, and the radical propagates rapidly. Long polymer chains are now obtained. The synthesis eventually obtains a sufficient numbers of particles of a sufficiently large size, and newly formed radicals in the aqueous phase starts entering the pre-existing particles rather than nucleating new ones. Monomer is migrating into the particles, the average particle size increases and the polydispersity decreases. When all of the monomer has been consumed the polymerization has effectively ceased [Gilbert, 1995]. Through the synthesis the particles obtain adequate electrostatic surface potential to stabilize the suspension by electrostatic repulsion [Pashley and Karaman, 2004].

When the particles are prepared by a surfactant free emulsion polymerization method they have a surface charge generated by the initiator. When having V50 as initiator, the particles obtain a positively charged surface. Furthermore, the polar ends of the initiator are located at the surface of the particles, making the surface relatively polar [Gilbert, 1995].

3.2 The Particle Template

The investigations performed by Dimitrov and Nagayama (1996) concluded that it was possible to create a CP pattern using the TLFD technique. The growth of particle arrays in the investigation of Dimitrov and Nagayama (1996) required slow withdrawal rates. It could be interesting to investigate whether higher rates of withdrawal could be used, to optimise the assembling by making it faster. Therefore, the same TLFD technique as Dimitrov and Nagayama (1996) will be used, but under atmospheric conditions, room temperature, and without SDS on the surface of the substrates. This technique is used to utilize the lateral capillary forces in the attempt of making a CP particle area with a hexagonal lattice [Dimitrov and Nagayama, 1996]. Additionally, an electric field will be applied. It is expected, that an electric field can influence the packing of the particles, because the application of an electric field have been observed to be able to enhance the lateral capillary forces [Trau *et al.*, 1996].

3.2.1 Thin Liquid Film Deposition

An experiment using only the TLFD technique will be performed as a reference. Hereby, it is possible to investigate how many particles that reaches the substrate, and how they arrange on the surface, when using only the TLFD technique. In this way, an optimal PS concentration of particles and withdrawal rate can be estimated. Glass slides will be used as surface in this experiment, because of a limited number of metal pre-coated slides. The glass slides used for this experiments will be cleaned before use by soaking them into concentrated sulfuric acid and afterward a nitric acid solution [Mori, 2007]. This is done to remove possible organic substances and other impurities from the surface. Scanning Electron Microscopy (SEM) will be used to analyse the samples.

Polystyrene Suspensions and Withdrawal Rates

PS suspensions with concentrations around 5, 10, and 24 g/L will be prepared in accordance with the work done by Hanarp and coworkers (2003) and Abdelsalam and coworkers (2005). The withdrawal rates are chosen to be $6.7 \cdot 10^{-3}$, $3 \cdot 10^{-2}$, and $1 \cdot 10^{-1}$ mm/s with accordance to the work done by Dimitrov and Nagayama (1996).

Properties of the Metals

The wettability properties of the metals will be investigated, because this is important when using the TLFD technique [Dimitrov and Nagayama, 1996]. In the literature Cu, Al, and Cr are found to possess water CAs of 97°, 81° [Min and Webb, 2001] ,and 82±5°[Wang *et al.*, 1999], respectively. The CA of the metals will be measured and additionally, the water CA will be measured for the cleaned glass slides, which in the literature are found to possess a water CA of 20° [Mori, 2007]. Furthermore, an experiment using only the TLFD technique and metal substrates will be performed to investigate the response of the metal surfaces to this technique. This is the reference sample for the "Application of an Electric Field" investigations. SEM will be used to analyse the respond of the metal surfaces to the TLFD technique.

3.2.2 Application of an Electric Field

When the TLFD technique is applied an electric potential, the electric potential will be provided and controlled by a potentiostat. The potentiostat regulates the current to keep a constant electric potential between the working and reference electrodes [Harris, 2002]. Glass slides pre-coated with metals (Cr, Al, and Cu, recieved from Teknologisk Institut in Århus) will be used as substrate (working electrode, WE), a Pt wire will be used as counter electrode (CE), and a calomel electrode will be used as reference electrode (RE). The substrate (WE) and the calomel electrode (RE) will be placed as close to each other as possible. The set-up of electrodes is illustrated in Figure 3.4. Furthermore, the set-up can be seen in Appendix C.

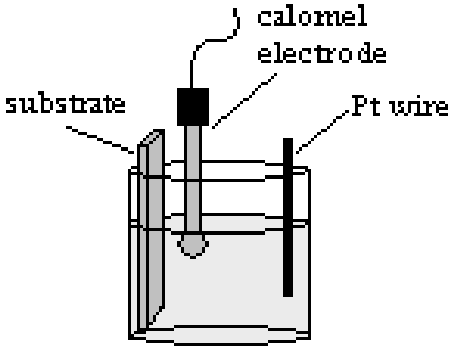

Figure 3.4: The electrochemical set-up. The experiments will be performed in a plastic beaker. The plastic beaker contains a PS suspension. At the left a glass slide pre-coated with metal is placed (WE), in the middle, a calomel electrode (RE), and at the right a Pt wire (CE). The substrate will still be withdrawn from the suspension by the "Dipper".

In this experiment, it will be attempted to let the particles move primarily by Brownian motions and the forces and flux from the TLFD technique. Therefore, the electric field applied should be a weak electric field, so the forces, that a field would normally exert on the particles, is almost negligible. Note, the field is applied to retain the PS particles on or repel them from the substrate, not to migrate the particles toward the substrate. A weak electric field is achieved when applying 500 mV, and therefore voltages in the range of 0 - 500 mV will be investigated. The analysis of the surfaces will be by SEM, and furthermore current measurements will be collected.

3.3 Sputter Coating and Particle Removal

After deposition of the particles on the surface, the surface will be sputter coated with a metal. The metal will in these investigations be Au, because Au is sputter coated onto the surfaces before SEM analysis. When the substrate with the template has been sputter coated, the particles will be removed. Different methods of removing the particles will be investigated.

First, it will be investigated whether a heating of the sample can remove the particles. The samples will be heated up to 550°C for two hours, because this temperature is known to destroy organic materials without loosing larger amounts of inorganic material [DSA, 1980].

Another method, that will be investigated in the attempt of removing particles from the gold coated surface, is a washing method, were the surface will be washed in an organic solvent to dissolve the particles. The surface will in these investigations be washed with toluene, because of the chemicals known ability of quickly dissolving PS.

Finally, a method involving sonication of the sample for 5 minutes in toluene will be investigated. The application of ultra sound is known to fragment macromolecules and have been used for mixing, solubilization, driving chemical reactions etc. [Soanes and Stevenson, 2005; Wang *et al.*, 2008; Hlavac and Rouer, 1997].

The results of the removal investigations will be verified by SEM.

3.4 Problem Statement

From the ideas presented in the experimental design, following problem statement will be investigated:

Is it possible to achieve a nanostructuring of metal surfaces using polystyrene particles as template?

This gives rise to following questions:

1. Is it possible to obtain an arrangement of CP particle mono-layer with a hexagonal lattice using positively charged polystyrene particles and metal surfaces?
2. Can the self-assembly of the particles be controlled or enhanced when applying an electric potential on the surface in a thin liquid film deposition process?
3. Can the particles be removed from the surface after coating, leaving a nanostructured surface?

Chapter 4

Interaction Forces

Different forces can be expected to interfere when depositing particles onto the substrates. In this chapter, the forces acting between surfaces in the PS suspension are therefore examined. Particle-particle and particle-flat surface interactions will be present in the suspension. Thus, the DLVO theory and the non-DLVO forces are described. Furthermore, the influence of surface roughness on the van der Waals and electrostatic forces will be mentioned. The term "particle" are in this and following chapters defined as spherical particles.

4.1 DLVO-Theory

When working with a colloidal suspension the particles are electrostatic stabilized. This is caused by the fact, that most solids release ions to some extend when immersed in a high dielectric liquid such as water. This is caused by dissociation of ions from the surface. The dissociated ions will be of high density, which will induce repulsive forces between the equally charged ions. Furthermore their will be a strong attraction between the dissociated ions and the surface [Pashley and Karaman, 2004]. Therefore, the charges on the surface is balanced by the dissociated ions, where some of the ions are bound to the surface and form the Stern layer. The remaining ions form a diffuse electric double layer in the liquid close to the charged surface. In this layer electrostatic attractive forces pull the ions toward the surface and entropic forces pushes the ions apart from each other and away from the surface to increase the entropy [Mate, 2008].

This diffusive layer of ions is also present when immersing glass substrates in water because the glass surface hydroxylates, as given in Equation (4.1) [Mate, 2008].

$$\mathrm{SiOH} \longrightarrow \mathrm{SiO^-} + \mathrm{H^+} \tag{4.1}$$

4.1.1 Particle-particle Interactions

When to surfaces with similar charge approaches each other in a liquid, their electric double layer starts to overlap. This increases the ion concentration near the surface, which leads to

an decrease in entropy and an entropic repulsive interaction is generated [Mate, 2008]. Besides the electric double layer force, long-range van der Waals forces, that are always attractive, are always present between two the surfaces [Pashley and Karaman, 2004].

In the DLVO theory, the total potential energy is expressed as the sum of the attractive (V_A) and repulsive (V_R) potential energy (Equation 4.2) [Hamley, 2006].

$$V = V_R + V_A \tag{4.2}$$

where the repulsive force, for a particle-particle interaction, when having a constant potential, a diffusive layer at size of the particle radius, and particles of equal radii, is given by Equation (4.3) [Goodwin, 2004].

$$V_R = 2\pi\epsilon_r\epsilon_0 a\psi_\delta^2 exp(-\kappa H) \tag{4.3}$$

or with constant potential and a thin diffusive layer (Equation 4.4)[Goodwin, 2004].

$$V_R = 2\pi\epsilon_r\epsilon_0 a\psi_\delta^2 ln\left[1 + exp(-\kappa H)\right] \tag{4.4}$$

where H is the distance between the surfaces, κ is the Debye-Hückel screening length, ϵ_r is the relative permittivity, ϵ_0 is the vacuum permittivity, a is the radius of the particle and ψ_δ is the surface potential. When the particles are of the same radii, the attractive force is given by Equation (4.5) [Goodwin, 2004].

$$V_A = -\frac{A}{12H}\left[1 + \frac{H}{2a+H} + \frac{H}{a} ln\left(\frac{H}{2a+H}\right)\right] \tag{4.5}$$

where A is the Hamaker constant, that is a function of both the electronic polarisability and the density of the material. The attractions between particles in a medium is weakened due to an additionally attraction with the medium. The attractive potential should therefore be calculated as the geometric mean of that of the particle ($A_{particle}$) and that of the medium (A_{medium}) with respect to their values in vacuum. The Hamaker constant is given by Equation (4.6) [Eastman, 2005].

$$A = \left(\sqrt{A_{particle}} - \sqrt{A_{medium}}\right)^2 \tag{4.6}$$

The repulsive potential is due to overlapping electrical double layers and the attractive potential is due to van der Waals forces [Hamley, 2006]. For a stable suspension the plot of the potential energies can look like given in Figure 4.1.

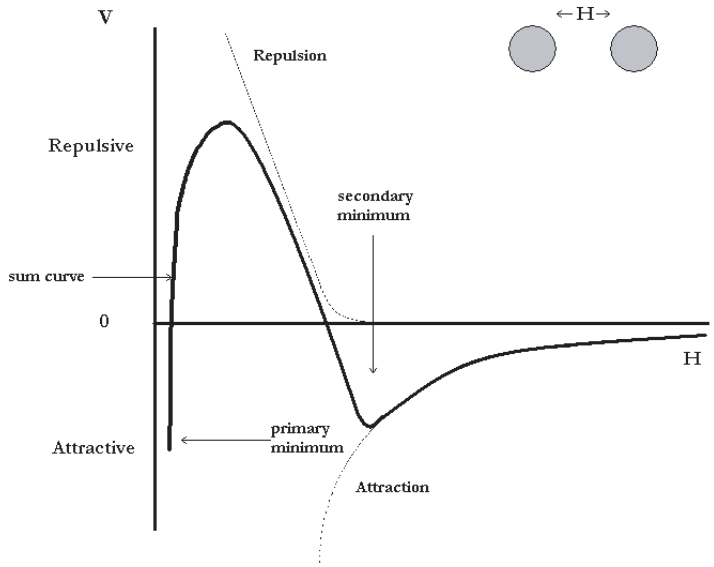

Figure 4.1: An example of the plot of the potential energies, and the sum curve, as a function of the distance between two particles for a stable suspension [Pashley and Karaman, 2004].

The colloidal suspension will in this example be stable because of the large kinetic barrier, that has a higher potential than in the primary minimum. The lowest potential is found in the primary minimum [Hamley, 2006].

4.1.2 Particle-plate Interactions

The interactions between two equally sized particles do not equal the interactions between a particle and a plate. The particle-plate repulsive potential energy is given as Equation (4.7) [Goodwin, 2004].

$$V_R = 4\pi\epsilon_r\epsilon_0 a\psi_\delta^2 exp(-\kappa H) \tag{4.7}$$

for κ a < 5 at weak overlap. At close approach the repulsive potential is given by Equation (4.8) [Goodwin, 2004].

$$V_R = 4\pi\epsilon_r\epsilon_0 a\psi_\delta^2 ln\left[1 + exp(-\kappa H)\right] \tag{4.8}$$

This repulsive force described above is when assuming the surface potential of the particle and the plate to be equal. This is not believed to be the case of the system in this work. From the cite [Goodwin, 2004] a repulsive force describing when a particle (with radius a_1) interacts with another particle (with radius a_1) and the two surfaces have different surface potential, and is given by Equation (4.9) [Goodwin, 2004].

$$V_R = \frac{\pi\epsilon_r\epsilon_0 a_1 a_2}{a_1 + a_2}(\psi_{\delta 1}^2 + \psi_{\delta 2}^2)\left\{\frac{2\psi_{\delta 1}^2 + \psi_{\delta 2}}{\psi_{\delta 1} + \psi_{\delta 2}^2}\right\} ln\left[\frac{1 + exp(-\kappa H)}{1 - exp(-\kappa H)}\right] + ln\left[1 - exp(-2\kappa H)\right] \tag{4.9}$$

Assuming a_1 to be very small and hereby negligible, because a_2 is a much larger substrate, an expression like in Equation (4.10) could be an approximation of the repulsive forces between a particle and a plate of difference surface potentials, which is expected in this work.

$$V_R = \frac{\pi\epsilon_r\epsilon_0 a_2}{a_2}(\psi_{\delta 1}^2 + \psi_{\delta 2}^2)\left\{\frac{2\psi_{\delta 1}^2 + \psi_{\delta 2}}{\psi_{\delta 1} + \psi_{\delta 2}^2}\right\} ln\left[\frac{1 + exp(-\kappa H)}{1 - exp(-\kappa H)}\right] + ln\left[1 - exp(-2\kappa H)\right] \tag{4.10}$$

Equation (4.10) can be reduced to Equation (4.11).

$$V_R = \pi\epsilon_r\epsilon_0(\psi_{\delta 1}^2 + \psi_{\delta 2}^2)\left\{\frac{2\psi_{\delta 1}^2 + \psi_{\delta 2}}{\psi_{\delta 1} + \psi_{\delta 2}^2}\right\} ln\left[\frac{1 + exp(-\kappa H)}{1 - exp(-\kappa H)}\right] + ln\left[1 - exp(-2\kappa H)\right] \tag{4.11}$$

The attractive forces are given by Equation (4.12) [Goodwin, 2004].

$$V_A = -\frac{Aa}{6H} \tag{4.12}$$

Both the repulsive and attractive force in the particle-plate interaction, when disregarding the approximation of the repulsive forces (Equation 4.11), is twice that of two similar spherical particles [Goodwin, 2004].

4.1.3 Surface Roughness

Surface roughness of material is stated to affect the van der Waals and the electrostatic interactions. Surface roughness have been observed on glass, PS, and acrylic particles ranging from 43 to 6350μm in diameter [Suresh and Walz, 1996]. By assuming to have a rough particle and a smooth surface, both with a surface potential of 50 mV, the forces can be modeled. When modeling the attractive van der Waals forces as a function of the surface roughness, it has been found that the van der Waals forces increase with increasing asperity size (surface roughness) (asperity radius of 0 nm, 20 nm, 30 nm, and 40 nm were used). Hence, the van der Waals attraction is larger at larger separation distances. The influence of surface roughness on the electrostatic forces has been modeled at larger separation distances. Again the electrostatic forces increases with increasing asperity size (surface roughness) (asperity radius of 0 nm, 20 nm, 30 nm, and 40 nm were used)[Suresh and Walz, 1996].

When determining the effect of the surface roughness on the total interaction energy, it is observed that the increasing roughness lowers the depth of the secondary minimum and pushes the minimum to a larger separation distance. Additionally, at these larger separation distances an increasing electrostatic repulsion is achieved, as an effect of the surface roughness, and the particles are pushed further away from each other. Moreover, at smaller separation distances the asperities have a greater impact on the van der Waals forces, and the potential energy barrier is lowered substantially. The summary of this is, that the electrostatic forces are more sensitive to the asperities at larger separation distances than the van der Waals forces. At smaller distances, the reverse is true. A general effect of the roughness is that the secondary minimum is reduced and shifted toward a larger separation distance and the height of the primary repulsive energy barrier greatly lowered [Suresh and Walz, 1996].

4.2 Non-DLVO Forces

When two surfaces or particles approach closer than a few nanometers the theory of attractive van der Waals forces and repulsive electrostatic double-layer forces often fail to describe their interactions. This is either because one or both of these theories are not valid at small separations or because non-DLVO forces comes into play. The non-DLVO forces are also both attractive and repulsive forces and these forces can be much stronger than the DLVO forces at small separations [Israelachvili, 1995]. The particles in colloidal suspensions of PS are separated by water. Because water is a liquid with a high dielectric contant and a high degree of hydrogen bonding between the water molecules, it leads to some distinct forces; electrostatic double layer forces, hydration repulsion, and hydrophobic attraction [Mate, 2008]. The electrostatic double-layer force is the repulsive force that occur when double-layers overlap, and is similar to the force that is described in Section 4.1. Therefore, only hydration forces and hydrophobic attraction will be described in this section.

A strong network of hydrogen bonding exist between water molecules in bulk water. Therefore, when an surface is immersed into the water, the water molecules in the immediate vicinity rearrange themselves to obtain the most favorable interaction in their new situation, also when this rearranging entails an interfering with the hydrogen bonding between the water molecules. When the distance between two surfaces are a few molecular diameters, the water becomes further disrupted. This leads to either repulsive or attractive forces between the surfaces depending on whether the surface is hydrophilic or hydrophobic, respectively [Mate, 2008].

4.2.1 Hydration Repulsion

The precise nature of the hydration repulsion forces between two hydrophilic surfaces is still unclear. The repulsion is thought to be caused by water molecules adjacent to the surface, which is hydrogen bonding to the hydrophilic surface groups, such as hydroxyl (-OH) and with hydrated surface ions. Energy is needed to disrupt the hydrogen bonding network sufficiently, to squeeze water out from between two surfaces, that are approaching each other. The hydration repulsion energy is found to decay exponentially with the distance between the surfaces [Mate, 2008].

4.2.2 Hydrophobic Attraction

Hydrophobic surfaces repel water (water CA of $\geq 90°$), therefore, when two hydrophobic surfaces in water approach each other, the water is spontaneously repelled from between the surfaces when the separation is sufficiently small. The flight of the water molecules is associated with an attractive force (hydrophobic attraction) acting between the two hydrophobic surfaces. Also the hydrophobic attraction is found to decay exponentially with the distance between the surfaces [Mate, 2008].

At molecular level the nature of the hydrophobic attraction between surfaces is still unclear, as the nature of the hydration repulsion. But when looking at similar hydrophobic attraction between hydrophobic molecules dissolved in water, a hydrophobic attraction is seen because of the water molecules have difficulties of hydrogen bonding to the hydrophobic molecule. Instead the water

molecules form a hydrogen bonding network around the hydrophobic molecules, and hereby maximizes the hydrogen bonding between adjacent water molecules. This hydrogen bonding network has a more ordered structure in proportion to liquid water, and this entails a increase in free energy due to a reduction in entropy. When two hydrophobic molecules, which are surrounded with their structured water shells, come together, a decrease in free energy occur. This is caused by structured water molecules being released to a more disordered liquid bulk state. A similar effect is thought to be due to hydrophobic attraction between hydrophobic surfaces [Mate, 2008].

Another possible explanation of the hydrophobic attraction is that dissolved gas forms "nanobubbles" (bubbles of nanometer size) on the hydrophobic surface. When two hydrophobic surfaces are brought together the "nanobubbles" will coalesce to bridge the gap between the surfaces. The bubbles have a water CA $> 90°$ and therefore, this creates a meniscus that exerts an attractive force. This bubble bridging leads to a different much longer range type of hydrophobic attraction, than the one gained from the first explanation. Hydrophobic attraction induced by "nanobubbles" can appear at tens of nanometers separations [Mate, 2008].

Chapter 5

Experimental Methods

This chapter contains information about materials and methods used when synthesizing and characterizing PS particles. Furthermore, the materials, methods, and conditions used when depositing particles onto surfaces and testing the removal of particles from gold coated surfaces are described.

5.1 Synthesis and Characterization of Polystyrene Particles

500 mL deionized water, 0.3 mol/L styrene (>99%, Sigma-Aldrich Chemie GmbH, Steinheim, Germany) and 0.003 mol/L 2,2-Azobis(2-methylpropion-amidine)dihydrochloride (V50) (97%, Sigma-Aldrich Chemie, Steinheim, Germany) were used for the synthesis of PS. First, the inhibitor was removed from the styrene using a column containing glass wool and Al_2O_3 (anhydrous, Merck, Damstadt, Germany). A five-necked flask were placed in a water bath at 70 °C and most of the deionized water was added to the flask. The rest of the deionized water was used to dissolve the initiator. A gas flow of nitrogen was added to the flask, and the system was left for about 30 minutes. Styrene and the dissolved V50 were then added and the synthesis reacted overnight.

The PS particles was purified by filtrating the suspension three times through glass wool and hereafter 6 days of dialysis (12-14kDa, Medicell International Ltd, London) in deionized water (the water was changed every day). Afterwards, the size (Zetamaster S, Malvern instruments),and the zeta potential (Zetamaster S, Malvern instruments) of the particles were estimated. The concentration of the suspension was estimated by performing a dry weight measurement (after filtration and dialysis). A sample of the suspension was placed at 75 °C (Model: T5042E, Heraeus electronic, Kendro Laboratory Products) for two days (the dry weight measurements were performed in triplicate). The particle achievement was verified by SEM.

5.2 Deposition of Polystyrene Particles onto Surfaces

The deposition of particles onto surfaces was done first by using only the TLFD technique on glass slides (Microscope slides, 76×26mm, Knittel Gläser). From this an optimal rate and

concentration was estimated. These were used for the further investigations, where the TLFD technique was added an electric potential. Here metal pre-coated slides were used as WE.

5.2.1 Investigation of Optimal Rate and Concentration of Particles

Glass slides used for this experiment were cleaned before use, by first soaking them into concentrated sulfuric acid (95-97%, J.T. Baker, Malinckrodt Baker, Holland) overnight, then in concentrated nitric acid solution (62%, Bie & Berntsen AS, Denmark) for 7 hours. Afterward the glass slides were rinsed with deionized water. The glass slides was then stored in deionized water in a plastic beaker according to Mori (2007).

Thin Liquid Film Deposition

PS suspensions with concentrations of 5, 10, and 24 g/L were prepared. Glass slides were withdrawn from three different suspensions with three different withdrawal rates $6.7 \cdot 10^{-3}$, $3 \cdot 10^{-2}$, and $1 \cdot 10^{-1}$ mm/s using the "Dipper" illustrated in Figure 5.1. The "Dipper" is an apparatus, specially constructed for this project, that can withdraw slides vertical, and with different rates (details and a picture of the "Dipper" can be found in Appendix C). When using the "Dipper", the slide holder was placed so the slide was as close to the bottom of the "Dipper" as possible. A plastic beaker was placed below the slide. The suspension of PS particles was poured into the beaker, and the withdrawal of the slide was started immediately. The investigation was duplicated to see whether the results could be reproduced and the samples were analysed by SEM.

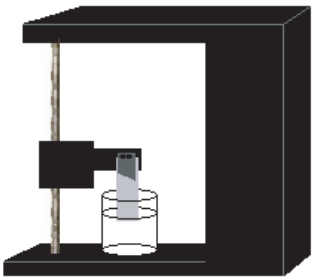

Figure 5.1: A sketch of the "Dipper" used to coat PS particles onto different surfaces.

Thin Liquid Film Deposition with metal as substrate

The response of the TLFD technique when using a metal pre-coated slide as substrate instead of a glass slide was tested. The metal pre-coated slide was withdrawn using the "Dipper", in the exact same way as when depositing particles on the glass slides. The optimal concentration of PS and withdrawal rate found in the previous experiment were used.

5.2.2 Application of an Electric Potential

Before the investigations of depositing PS particles onto the substrates using a combination the TLFD technique and an electric potential, the potentiostat was calibrated regarding the applied voltage and the current of the system. Afterwards, a test of the set-up was performed using a 20 g/L NaCl (99.5%, BDH, AnalaR, VWR International Ltd, United Kingdom) solution in deionized water, a Cr substrate (as-received from Teknologisk Institut in Århus), a calomel electrode (Ref 401, calomel, Radiometer analytical S.A., France), and a Pt wire. The system was checked varying the voltage applied (through the Pt wire) to the system, and measuring the output voltage and current (between the substrate and the reference electrode) with a multimeter (Digital multimeter, DT 9201). The system was ventilated and the test was performed at room temperature (22°C).

When applying the potential to the TLFD technique, glass slides pre-coated with metals (as-received from Teknologisk Institut, Århus) were used. The optimal concentration of PS and withdrawal rate from the previous experiment (cf. "Subsection 5.2.1") were used, and voltage was applied to obtain a substrate surface potential in range from 0-300 mV.

Stability of the zeta potential of the particles

The PS suspension was applied an electric field several times, and therefore the zeta potential of the particles, in the PS suspension, was measured to test the stability. This was done by extracting 40 μL of the suspension from the beaker and this was diluted until a volume of 20 mL was achieved. The zeta potential of the suspension was measured in between the preparation of the samples, where the electric potential of the surface was varied from 0-300 mV.

5.3 Removal of Particles from the Gold Coated Surface

It was tested whether particles could be removed from samples sputter coated with Au from the SEM analysis.

Two samples were heated up (Model: K10, Scandia-ovnen AS, Denmark) in air, with a rate of 1000°C/hours until 550°C. The temperature was held constant at 550°C for two hours, and the samples were afterward slowly cooled down.

Two other samples were placed in a blue-cap flask with toluene (pure, Bie & Berntsen, Denmark). The slide was placed so the ends of the slide were supported by the inside of the flask and so the side of the slide, that was coated with both particles and Au, was facing the cap of the flask (as illustrated in Figure 5.2). A magnet was added to the flask to stir the liquid and the flask was closed. The slide was left in toluene, while the toluene was stirred for 43 hours. The sample was removed from the blue-cap flask and was placed in a fume hood for half an hour.

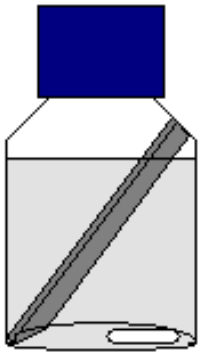

Figure 5.2: Sketch of the washing method, which was one of the methods tested for the ability of removing particles from the surfaces.

Finally, two samples were placed in a blue-cap flask with toluene, and the slide was again placed as previous described (illustrated in Figure 5.2). This time the blue-cap flask was placed in a sonicater (Output: 100 Watts, 42 kHz ± 6%)(Branson 2510, Branson Ultrasonics Corporation, USA), and the samples were sonicated for 5 minutes. The sample was removed from the blue-cap flask and was placed in a fume hood for half an hour.

All the samples were analyzed by SEM.

5.4 Scanning Electron Microscopy

Before the analyses by SEM (Zeiss EVO 60, Brock & Michelsen A/S, United Kingdom), the samples were coated (Model S150B sputter coater, Edwards, United Kingdom) with 20-30 nm of Au. The coating was a plasma coating. The samples were analyzed using EHT (earthed high tension): 4 kV when analyzing particle film deposited onto glass slides, and EHT: 6 kV when the particle film was deposited onto metal pre-coated slides. Furthermore, the images taken were all with a magnification of 5000 (unless otherwise stated) to ease the subsequent comparison of the samples. When characterizing the metal surfaces and their respond to the TLFD technique, the samples were not sputter coated with gold, and therefore EHT: 4 kV was used. Also the samples from the "Removal of Particles from the Gold Coated Surface" test (Section 5.3) were analyzed using EHT: 4 kV. The samples were analyzed by taken approximately 10 images at random places at the sample.

5.4.1 Average Particle Area Fraction

The average particle area fraction was estimated using the picture analysis program "ImageJ 1.38x". This was done by first extracting the area of the picture above the toolbar, because this would interfere in the analysis (Rectangular selections, image → crop). Then, the background was subtracted (Process → Subtract Background (radius 15, marking from "Light B" is removed)). Furthermore, also a filter was used to improve the analysis (Process → Filters → Median (radius 2)). The area fraction on the picture was found by adjusting the threshold so only the particles were represented (Image → Adjust → Threshold). The area fraction was measured (Ctrl + M).

5.5 Contact Angle

The CA measurements were manually performed by placing a droplet of water to the concerned surfaces and take a picture (Image Point, Photometrics, Korea). The pictures were taken about 1 minute after the droplet was placed, to ensure that equilibrium state was achieved. When measuring the CA of the glass slides (the more hydrophilic surfaces) 5 μL deionized water was used. 6.5 μL deionized water was used when measuring the CA of the metal surfaces (the more hydrophobic surfaces). Furthermore, the measurements were performed under atmospheric pressure and room temperature. The CAs (θ) were calculated from Equation (5.1).

$$\theta = \left[\pi - 2\left(atan\left(\frac{DW}{2 \cdot DH}\right)\right)\right] \cdot \frac{180}{\pi} \tag{5.1}$$

DW is the drop width and DH is the drop height, and these parameters were estimated from the images using "ImageJ 1.38x" as illustrated in Figure 5.3.

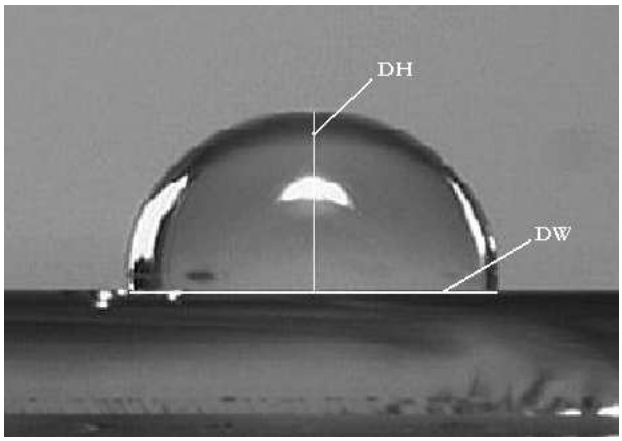

Figure 5.3: An example of a CA measurement image, where the width (DW) and the height(DH) measured, using "ImageJ 1.38x", are marked at the image.

Chapter 6

Results

This chapter is divided into five parts. First, the characterization of the particles synthesized for preparation of the particle template. Second, investigations of depositing particles onto glass surfaces using the TLFD technique. Third, characterization of the metal pre-coated surfaces, which were used when an electric potential was applied. Fourth, application of an electric potential to the TLFD technique. Finally, removal of the particles after the template have been coated with gold. The results will be presented and partially discussed.

6.1 Characterization of Polystyrene Particles

Two Surfactant free emulsion polymerizations of styrene were performed and PS particles were obtained, as seen in Figure 6.1.

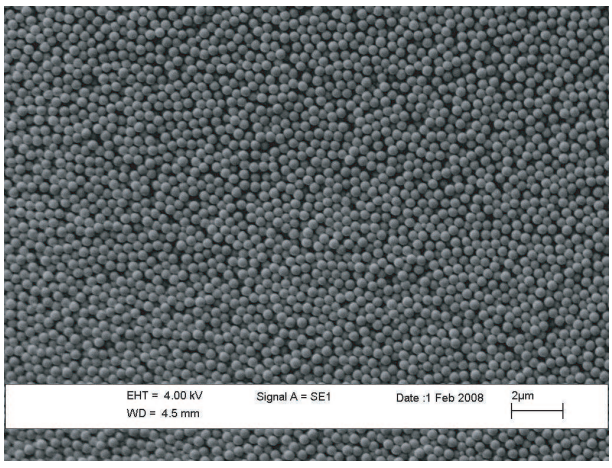

Figure 6.1: SEM image of particles from batch 1.

Size and zeta potential of the two batches were measured and the results are given in Table 6.1. It was desired to obtain batches of particles with the same average size to ease the comparison of the later results. The two batches prepared contained particles with an average size around 400 nm, and the small differences in average size should not have an influence on the properties

of the resulting modified surfaces. If CP particles with a hexagonal lattice are achieved, the template will give a solid fraction of 0.093, no matter what size the particles posses. Moreover, the particles were observed to posses a positively charged surface, which was also expected when using V50 as initiator. The batches had different zeta potentials, however, the influence of this difference can be avoided if particles from the same batch are used for the same investigation. The number of the batch used in the investigation will be stated before each investigation.

Table 6.1: The size, zeta potential, and concentration of the PS particles in the different batches. Furthermore, the standard deviation is given.

Batch number	Average size [nm]	Zeta potential [mV]	Concentration [g/L]
1	418 ± 9	66 ± 2	24.47
2	392 ± 3	55 ± 2	28.77

6.2 Withdrawal Rate and Polystyrene Concentration

It was from this investigation attempted to find the optimal rate of withdrawal of the substrate and optimal concentration of particles in the suspension, from which the substrate was withdrawn. Furthermore, it was investigated whether it was possible to obtain a CP mono-layer, as obtained by Dimitrov and Nagayama (1996), when the evaporation from the film was not controlled and no modification was performed on the glass slides prior to the deposition of particles. Three different rates and three different concentrations were chosen, and glass slides were used as substrate. The samples were withdrawn from suspensions made from batch 1. The designations of the samples are given in Table 6.2.

Table 6.2: The samples prepared for the investigation of optimal rate of withdrawal of the substrate and optimal concentration of particles. The samples will be designated in the text as seen in the table. Thus, sample A5 is withdrawn with a rate of $6.7 \cdot 10^{-3}$ mm/s and is withdrawn from a 5 g/L suspension of PS particles. The suspensions were prepared from batch 1.

Rate [mm/s]	Concentration [g/L]		
	5	10	24
$6.7 \cdot 10^{-3}$	A5	A10	A24
$3 \cdot 10^{-2}$	B5	B10	B24
$1 \cdot 10^{-1}$	C5	C10	C24

The investigation was duplicated to see whether the results could be reproduced. The results were reproducible as the same tendencies were observed from the two independently performed experiments. The SEM images can be found on the Enclosure CD - "Results" - "Investigation of Rate and Concentration".

When the samples were withdrawn from the suspension, a dull white layer was observed at all slide surfaces. Moreover, the film seemed relatively homogeneously distributed on the surface. From the SEM analysis it was verified that particles were adsorbed onto all the glass slides. Furthermore, the particle film was present at both sides of the slide. All samples showed a little opalescence, which was observed as mostly green colors dependent on the angle the slide was held in. The opalescence is due to a systematic packing of particles. The opalescence was especially distinct for sample A24, and A10 showed a little more opalescence than the rest of the samples. When analyzing sample A24 by SEM, a more systematically packing of the sample was observed, which can be seen in Figure 6.2, A24 image 2. The formation of a systematically packed layer seemed to be caused by multi-layering of the particles.

The SEM analysis of samples A5 showed areas of mono-layers with particles distributed with large distances between the particle aggregates. The average area fraction of particles in mono-layer was 31 %± 9% (Figure 6.2, A5 2). Furthermore, some areas with multi-layers were observed at the sample (Figure 6.2, A5 1). The analysis of sample A10 showed also particles that were widely distributed in a mono-layer on the surface. However, the average area fraction of particles was 35% at sample A10, and hereby the area fraction was larger than on sample A5. Particle multi-layers were only observed on sample A10 in one of the experiments (Figure 6.2, A10). On the surface of sample A24 only large areas of multi-layers were observed (Figure 6.2, A24).

All samples withdrawn with $6.7 \cdot 10^{-3}$ mm/s showed multi-layers, which can be caused by the slow withdrawal rate. The particles are in this TLFD technique primary led to the sample by Brownian motion and the water flux toward the slide during withdrawal of the slide. When withdrawing the slide slowly, it could be possible that more particles have time to reach the slide, which explain the formation of multi-layers. In that respect, it would have been expected that sample A10 would have shown multi-layer areas in both of the independently performed experiments. The images of the samples were taken at six random places on the sample. Therefore, it is likely that multi-layers were present on both of the A10 samples, but just not observed when analyzing the sample. Maybe, also more widely distributed particle areas were present at sample A24, but was not observed. The particle concentration used when preparing sample A24 was 24 g/L. Accordingly, it is likely that more particles had adsorbed to sample A24 given primary areas of multi-layers. Nevertheless, it was distinct from the analysis, that the PS concentration has an influence on the samples, and that sample A24 contained larger and more areas of multi-layers than sample A5 and A10.

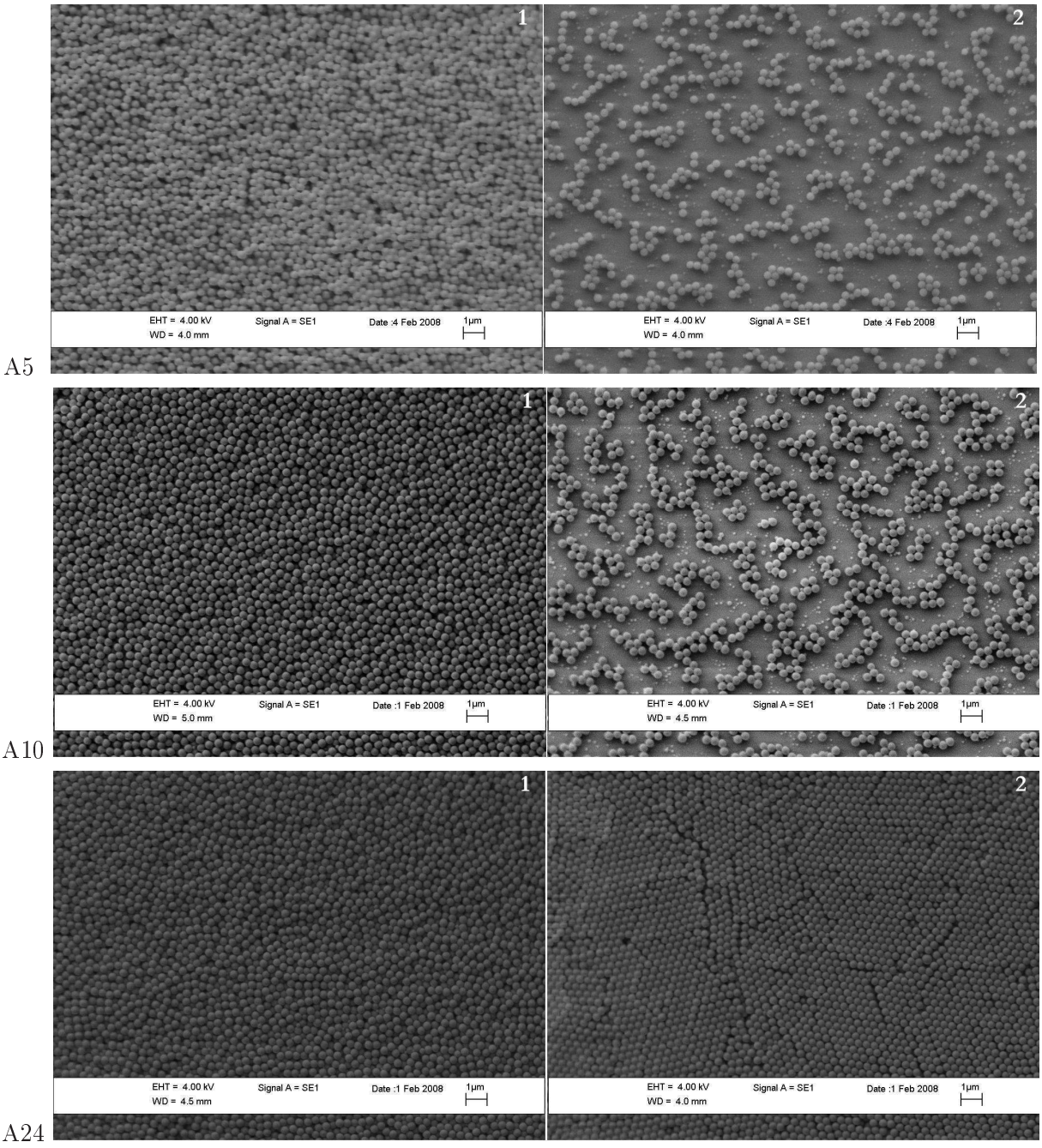

Figure 6.2: SEM images of the deposition of particles onto glass substrates using the TLFD technique. The samples withdrawn with $6.7 \cdot 10^{-3}$ mm/s (designated A) from suspensions with three different PS concentration (batch 1); 5, 10, and 24 g/L. The rest of the images can be found on the Enclosure CD - "Results" - "Investigation of Rate and Concentration".

Sample B5 was found to have mono-layers with an average particle area fraction of 27 %± 11%, which was a lower particle area fraction than the one observed on sample A5. No multi-layers were present at sample B5 (Figure 6.3, B5). Sample B10 had mono-layers with a average particle area fraction of 28 %± 3%, which was also a lower fraction than the particle area fraction on sample A10 (Figure 6.3, B5 1). Furthermore, double-layers were observed in one of the samples of B10 (Figure 6.3, B10). Again, randomly taken images could be the reason of this difference

between the B10 samples. Sample B24 had the most dense particle distribution in mono-layer of the samples withdrawn with $3 \cdot 10^{-2}$ mm/s, and the mono-layers obtained by the rate of $6.7 \cdot 10^{-3}$ mm/s. Thus, it had a average particle area fraction of 40 %$\pm$ 2% (Figure 6.3, B24 2). Furthermore, double-layers that shifted into mono-layers were observed at sample B24 (Figure 6.3, B24 1).

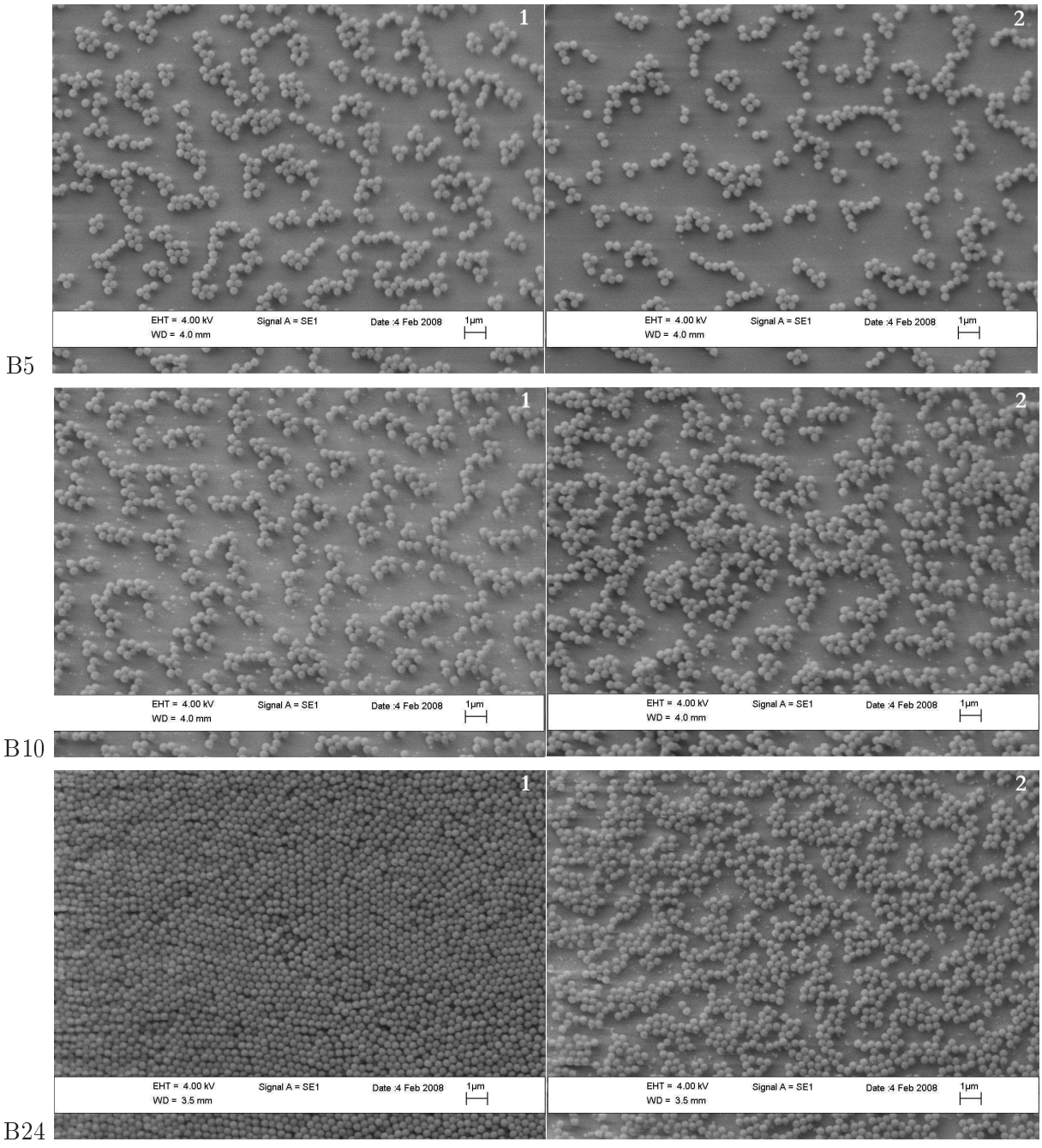

Figure 6.3: SEM images of the deposition of particles onto glass substrates using the TLFD technique. The samples withdrawn with $3 \cdot 10^{-2}$ mm/s (designated B) from suspensions with three different PS concentrations (batch 1); 5, 10, and 24 g/L. The rest of the images can be found on the Enclosure CD - "Results" - "Investigation of Rate and Concentration".

Sample C5 had mono-layers with an average particle area fraction of 21 %± 4%, and hereby less particles adsorbed in the mono-layer than sample A5 and B5. No multi-layers were observed at this sample. This can be due to the higher rate of withdrawal (Figure 6.4, C5). Sample C10 had mono-layers with an average particle area fraction of 28 %± 5% (Figure 6.4, C10).

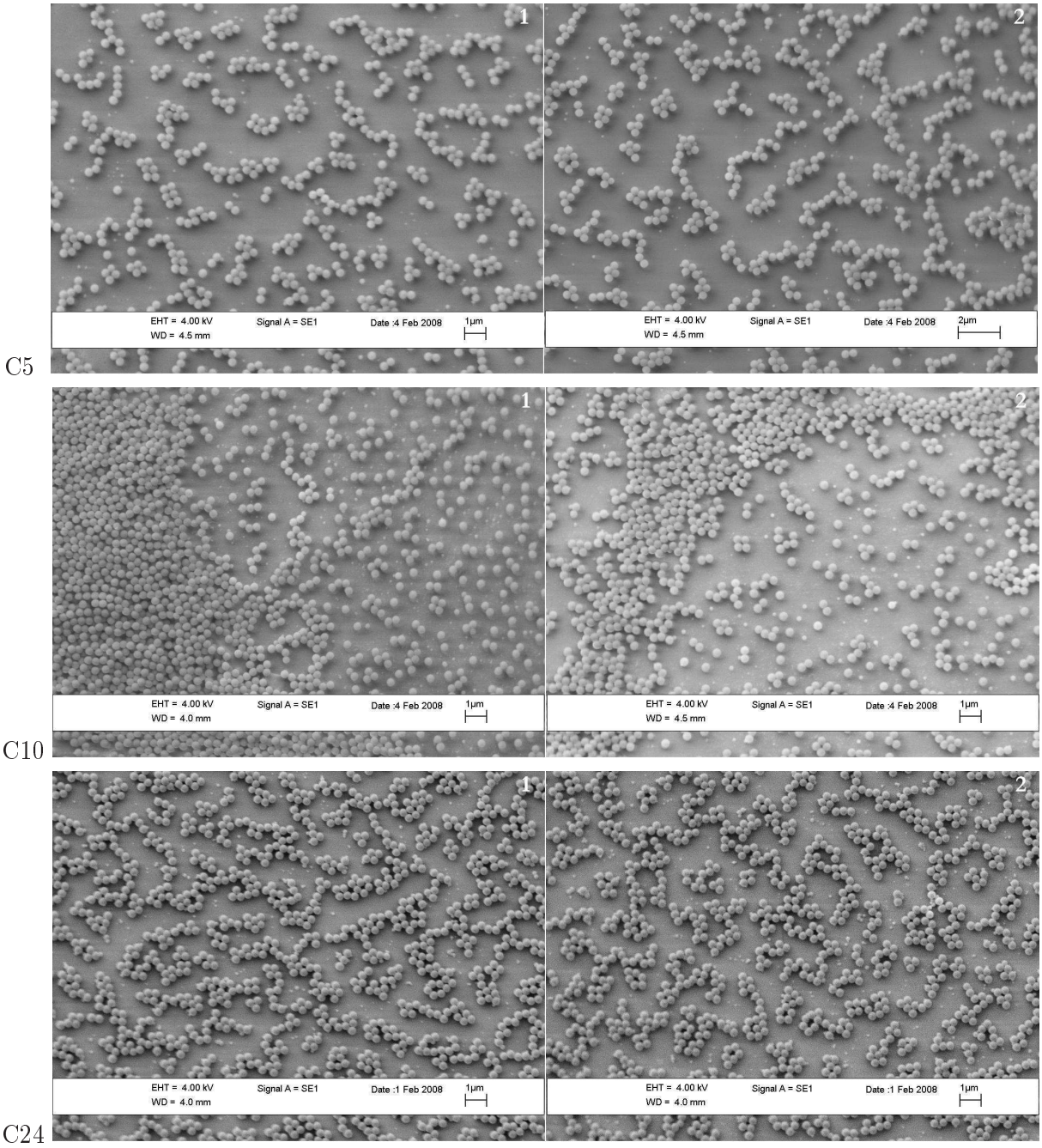

Figure 6.4: SEM images of the deposition of particles onto glass substrates using the TLFD technique. The samples withdrawn with $1 \cdot 10^{-1}$ mm/s (designated C) from suspensions with three different PS concentrations (batch 1); 5, 10, and 24 g/L. The rest of the images can be found on the Enclosure CD - "Results" - "Investigation of Rate and Concentration".

Furthermore, a phenomenon not seen at the other samples was observed at sample C10. Large areas were found, where the particles were not equally distributed on the surface as seen from

the mono-layers at the other surfaces. Instead particles lay close together, and with large almost particle-free areas around it. This could be because of the faster rate of withdrawal destroying the progress of the film. It was not seen at the other samples withdrawn with the same rate, therefore the phenomenon can be a result of the exact combination of rate and PS concentration (Figure 6.4, C10). Accordingly, the phenomenon would maybe be observed again if investigating more combination. Sample C24 was found to have a particle area fraction of 34 %± 5%, and hereby a higher particle area fraction than sample C5 and C10. Double-layers were observed in one of the experiments, also. Sample C24 had a lower particle area fraction than sample B24 (Figure 6.4, C24). The average area fractions of the samples are summarised in Table 6.3.

Table 6.3: Summary of the measurements of the average particle area fractions on the glass substrates, The area fractions were found using "ImageJ". Six images were taken at six random places at the sample. Furthermore, it is stated if multi-layer and double-layer were observed.

Rate [mm/s]	Concentration [g/L]		
	5	10	24
$6.7 \cdot 10^{-3}$	31 ± 9% / multi-layers	35% / multi-layers	multi-layers
$3 \cdot 10^{-2}$	27 ± 11%	28 ± 3%/ double-layers	40 ± 2% / double-layers
$1 \cdot 10^{-1}$	21 ± 4%	28 ± 5%	34 ± 5% / double-layers

In spite of both multi-layers and mono-layers on some of the samples the film deposition seemed much uniform. The same tendencies of shifts between mono-layers and multi-layers were observed on many of the samples and the particle mono-layers on the samples seemed to be equally distributed on the surface area. It was observed that a higher withdrawal rate, contributed to less particles being deposited on the surface. Moreover, a higher PS concentration, contributed to more particles being deposited onto the surface, as expected.

For further investigations it is chosen to continue the work with two of the combinations of withdrawal rate and PS concentration. Sample B24 was the sample which came closest to the desired surface adsorption, because it was observed to have the mono-layer with the highest particle area fraction (cf. Table 6.3). Therefore, the withdrawal rate of $3 \cdot 10^{-2}$ mm/s and a PS concentration of 24 g/L will be used in further investigations. There was also observed double-layers at this sample. However, the further investigation will entail an electric potential, and if this investigation is interpreted as an indication of how many particles that reach the surface with the given rate and particle concentration, there should be enough particles to cover the hole surface. Therefore, it is hoped that the application of potential to the substrate, and hereby an electric field in the system, eliminates the double-layers. This should of course be in an appropriate way, by filling out the empty places by rearrangement of the present particles. The particles will to some extend be affected by the electric potential. This is of course dependent on the strength of the applied field, and at some strength the influence can be almost negligible. If applying a positive potential to the substrate, particles could be repelled from the surface, therefore, a concentration and rate where double-layers could be formed would be suitable. If a negative potential is applied, the particles would move towards the substrate. Furthermore, the an electric field is known to enhance the lateral capillary forces. Again, this is dependent on the strength of the field. If the lateral capillary forces are enhanced from the used field strength,

the lateral capillary forces could be expected to be enhanced between particles at the substrate, and between particles at the substrate and in the surrounding liquid. Therefore, it is chosen also to do further investigations using sample C24, withdrawn with $1 \cdot 10^{-1}$ mm/s and from a PS concentration of 24 g/L. At this combination of concentration and rate, mostly mono-layers were observed and with an average particle area fraction of 34% ± 5% (Tabel 6.3). Hence, if more particles are led to the substrate, it might be better to have a substrate with less multi-layers and with room for migrating particles.

6.2.1 Vertical Surface Investigation of the Polystyrene Particle Film

In the previous investigations many of the samples were observed to have both areas of particle mono-layers and areas of particle multi-layers. It was then desired to know whether the mono-layer areas was primary present at the top and the multi-layers primary present nearer the bottom of the slide. Thus, this could be due to the slide surface nearer the bottom being immersed for a longer time, than the top of the slide. Therefore, sample B24, which was observed to contain mono-layers and double-layers, was analyzed by SEM, finding what seemed to be the top of the film, which was then the starting point (length = 0 mm). Then an image was taken at every 3 mm in vertical direction. The images will not be shown here (the images can be seen on the Enclosure CD - "Results" - "Vertical Surface Investigation of the Film"), but instead the observed layers will be described and displayed in Table 6.4. When talking about mono-layers and double-layer, the images will be approximately similar to the images shown in Figure 6.3, where a mono-layer is seen at image 2 and double-layer is seen at image 1. An illustration of the analyse method is seen beside the table.

The mono- and double-layers are not located primary at the top or at the bottom of the slide. Therefore, this will not be a problem in later experiment. In addition, this makes the sample even more appropriate for the further investigation. When having both not adequately packed mono-layers and double-layers, particles from the double-layers should be able to fill out the empty places at the slide. This is attempted by applying an electric potential, which could be able to rearrange the particles at the slide. Horizontal lines were observed at sample A5-A24 and B5-B24. Hence, these horizontal lines is also seen at the image illustrating the analysis of the surface. Therefore, the same shift between layers are most likely to occur in the other samples were the horizontal lines were observed. Furthermore, no horizontal lines were observed at the samples C5-C24, and the SEM analysis showed primarily mono-layers (cf. Section 6.2). This indicates that the horizontal lines observed on the surfaces are due to shifts between mono-layers and multi-layers or between multi-layers of different magnitudes.

Table 6.4: A vertical investigation of sample B24 performed by taken images from the top and down. The starting point was made where the film was assumed to start (length = 0 mm), and then images were taken every time the focus was moved 3 mm in vertical direction and until the bottom. When both mono- and double-layer are written at the same length, it means that a shift from mono-layer to a double-layer is observed at the image. An illustration of the analysis of the surface is seen at the left of the table.

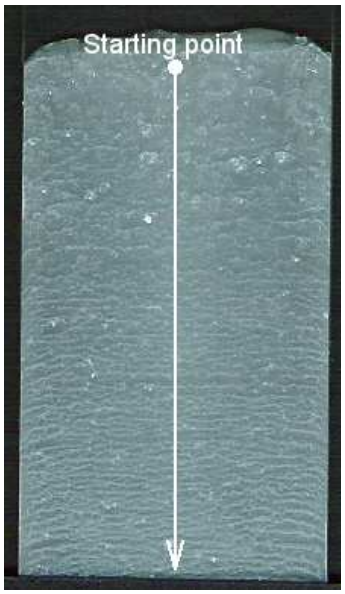

Length [mm]	layer
0	mono
3	mono
6	mono
9	mono
12	mono/ double
15	double
18	mono/ double
21	mono
24	double
27	double
30	double
33	mono
36	mono
39	mono
42	mono/ double
45	mono

6.3 Characterization of the Metal Surfaces

A metal surface will be used when applying an electric potential to the TLFD technique. Therefore, the wettability of the metals were investigated. Cu, Al, and Cr surfaces were in this work candidates when attempting to modify the surfaces. Additionally, an experiment using the TLFD technique on the metals without applying a potential was performed. From this the respond of the metal surfaces to this technique in proportion to when using glass surfaces were observed. In connection to this, CA measurements of a glass slide (cleaned according to Mori (2004)) were performed.

6.3.1 Contact Angle Measurements

The Cr surface was observed to possess the highest water CA, Al the second highest CA, and Cu possessed the lowest water CA. The theoretical and measured water CA of the different surfaces can be seen in Table 6.5. Moreover, images from the analysis can be seen in Figure 6.5. The CAs found for Cu and Cr deviated from the theoretical value with 13% and 16%, respectively. This are relatively high deviation in proportion to the CA measurement of the Al surface, that deviated with 5% from the theoretical value.

Table 6.5: Theoretical and measured water CAs of the metal surfaces and a glass substrate cleaned according to Mori (2004). The pictures were taken when the droplet was in equilibrium state. "ImageJ" was used to estimate the CAs.

Sample	Theoretical CA [°]	Measured CA [°]
Cu	97	84 ± 7
Al	81	85 ± 7
Cr	82	95 ± 12
Glass	20	20 ± 12

From the CA measurements, it was observed that the glass slide possessed a low CA and hereby was hydrophilic, in proportion to the metal surfaces, that were more hydrophobic, especially Cr (hydrophobic surface: CA $>$ 90 °). Therefore, the respond of the metal surfaces to the TLFD technique is expected to be different from the respond of the glass slide, according to Dimitrov and Nagayama (1996).

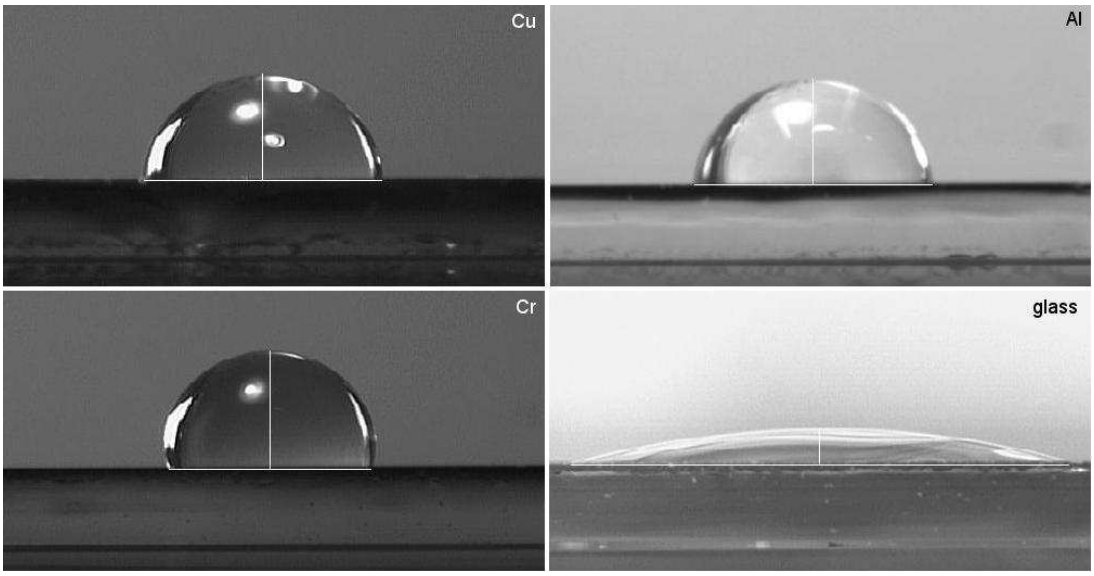

Figure 6.5: Images from the CA measurements of the Cu, Al, Cr and glass surface, respectively. The glass surface was before analysis cleaned according to Mori (2007).

6.3.2 Metal as Substrate in the Thin Liquid Film Deposition Technique

It was tested how the use of a metal substrate, instead of a glass substrate, influenced the particle deposition, when using only the TLFD technique. Different adsorption properties in proportion to the glass substrate was expected. It was observed, that a film of particles was deposited onto the three different metal surfaces, and that the film on the Al surface looked similar to the film deposited on the glass substrate. Furthermore, the film on the three different surfaces, seen in Figure 6.6, were observed to be different from each other.

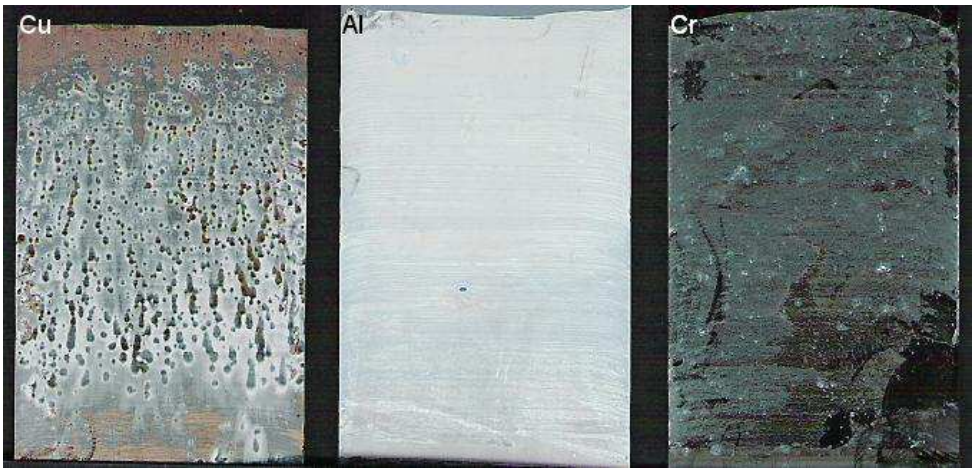

Figure 6.6: Particle deposition on Cu, Al, and Cr substrates using the TLFD technique. The metal pre-coated substrates were withdrawn from a 24g/L suspension of PS and with a rate of $3{\cdot}10^{-2}$ mm/s.

The film on the Cu surface was not homogeneously distributed. It seemed like the particles were more concentrated near the bottom of the slide than in the top of the slide (see Figure 6.6). When analyzing the surface, by SEM, primary large areas of particle multi-layers were observed, as seen in Figure 6.7 image 1. Furthermore, particle mono-layer areas with low particle area fraction were observed. Moreover, the Cu surface was observed to be planar as seen in Figure 6.7 image 2.

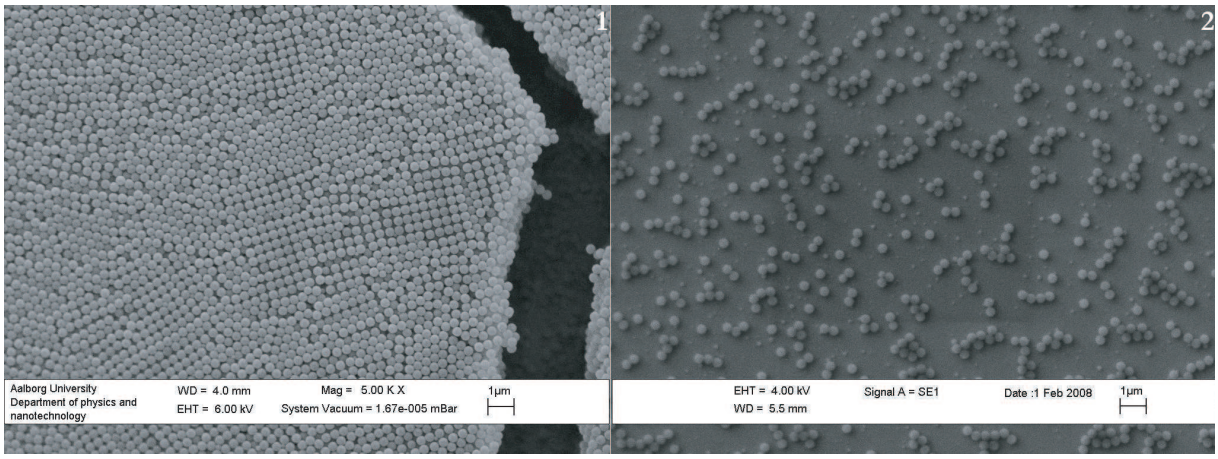

Figure 6.7: SEM image of a Cu pre-coated substrate withdrawn from a PS suspension of 24 g/L (batch 1) with a rate of $3{\cdot}10^{-2}$ mm/s. The rest of the images can be seen at the enclosure CD - "Results" - "Characterization of the Metal Surfaces".

The film on the Al slide was observed to be much similar to the films deposited on the glass slides (see Figure 6.6). When analyzing the sample by SEM, it was observed, that the particles were relatively equally distributed on the surface, like the particles on the glass surfaces (see Figure 6.8). However, the particles had not assembled in minor groups as seen on the glass surfaces. The relatively equally deposition of particles seemed to be due to the surface structure of Al. Unlike the planar Cu surface, the surface of the Al was more rough, and it seemed like metal pieces of about $1\mu m \times 1\mu m$ were present. Because the metal pieces are larger than the particles used for particle assembling, the metal pieces have a major impact on the applicability of Al for

deposition experiments. Thus, the metal pieces would hinder the assembling and thereby the CP of the particles.

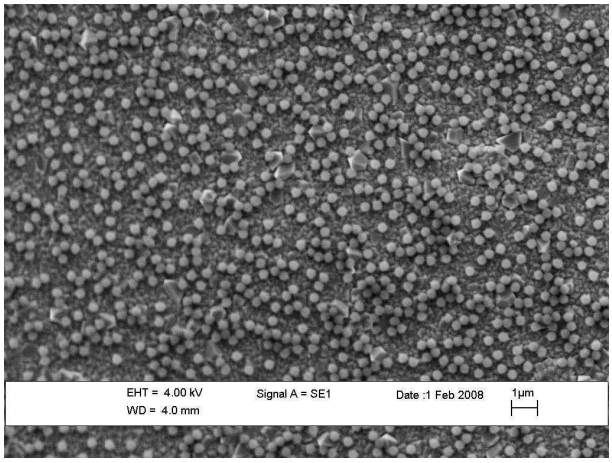

Figure 6.8: SEM image of an Al pre-coated substrate withdrawn from a PS suspension of 24 g/L (batch 1) with a rate of $3{\cdot}10^{-2}$ mm/s. The rest of the images can be seen on the Enclosure CD - "Results" - "Characterization of the Metal Surfaces".

The film on the Cr pre-coated substrate was also much similar to the film deposited on the glass slides. Although, it seemed like the film peeled of some places on the surface (see Figure 6.6). Furthermore, the film seemed thinner than on the Al, Cu, and the glass slides. When analyzing the sample using SEM, it was observed, that less particles had deposited on the surface, than on the Cu surface. Furthermore, mono-layers that were relatively closed packed were observed at many areas of the surface, as seen in Figure 6.9 image 1. This was also observed as a little opalescence on the surface. In addition, the Cr surface was observed to be porous, as seen in Figure 6.9 image 2. Thus, the surface was not rough like the Al surface, but had small holes, smaller than the particles. This porous surface could also be the explanation of the difference in the theoretical water CA and the measured water CA. Thus, roughening of a surface can contribute to a higher water CA (cf. Equation 3.1).

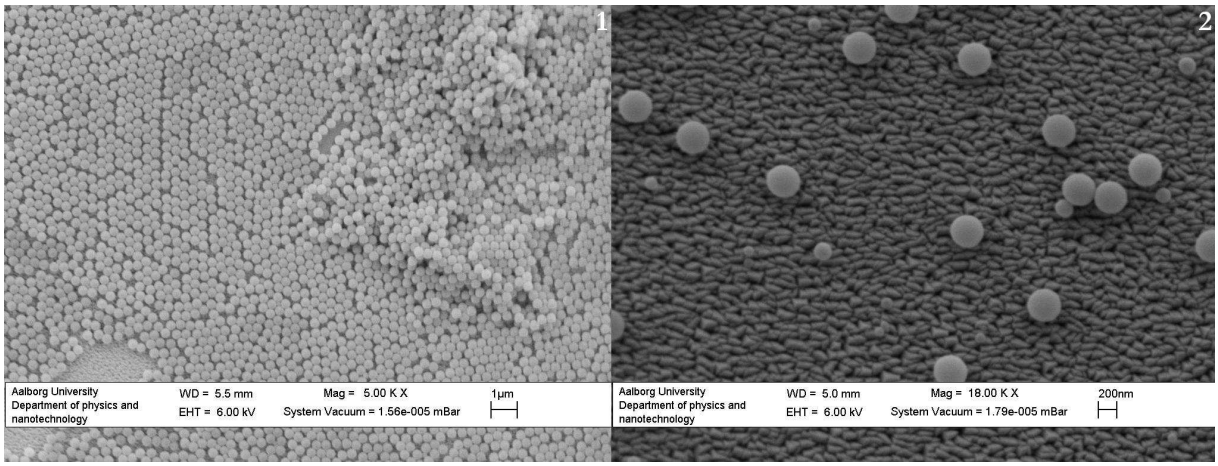

Figure 6.9: SEM image of a Cr pre-coated substrate withdrawn from a PS suspension of 24 g/L (batch 1) with a rate of $3{\cdot}10^{-2}$ mm/s. Image 2 has a larger magnification (18000) to make it possible to see the surface structure of the Cr substrate. The rest of the images can be seen at the enclosure CD - "Results" - "Characterization of the Metal surfaces".

The metal surfaces were observed to respond relatively different on the TLFD technique, than the glass slides. The differences in hydrophobicity/hydrophilicity could play an important role. Furthermore, the particle film was not as systematically deposited on the metal surfaces, as on the glass slides. The film on the metals was more heterogeneous. Additionally, the respond of the Al surface to the TLFD technique, is probably due to the rough surface structure. Because the rough surface would hinder the assembling of particles it is concluded, that the Al surface can not be used in further experiments. Hence, only the Cu and Cr surfaces will be used in further experiments. From the Cu sample it was observed that multi-layers were formed. Therefore, it is decided that the metal substrates will be applied a positive potential. Hereby, the particles will be repelled/pushed away from the substrate. The chrome reference did not contain the same amount of multi-layers, but seemed to contain mono-layers and double-layers. Still the chrome surfaces will also be applied a positive potential. Thus, to be able to determine an eventually effect of the potential application, when comparing the results from the different metal surfaces in the further investigations.

6.4 Application of an Electric Potential

The TLFD technique was added an electric potential using the substrate (metal surfaces) as a working electrode (cf. Subsection 3.2.2). Before the investigations could be started, a calibration of the potentiostat regarding voltage and current was performed (the calibration curves can be seen in Enclosure I). Furthermore, a test of the system was performed (see Figure 6.10). From this test it was seen, that the desired voltage that was applied (Voltage (set) [mV]) to the solution of sodium chloride was also the voltage measured between the substrate (WE) and the RE. This indicates that the system works, and the investigations of application of an electric potential to the TLFD technique can be performed.

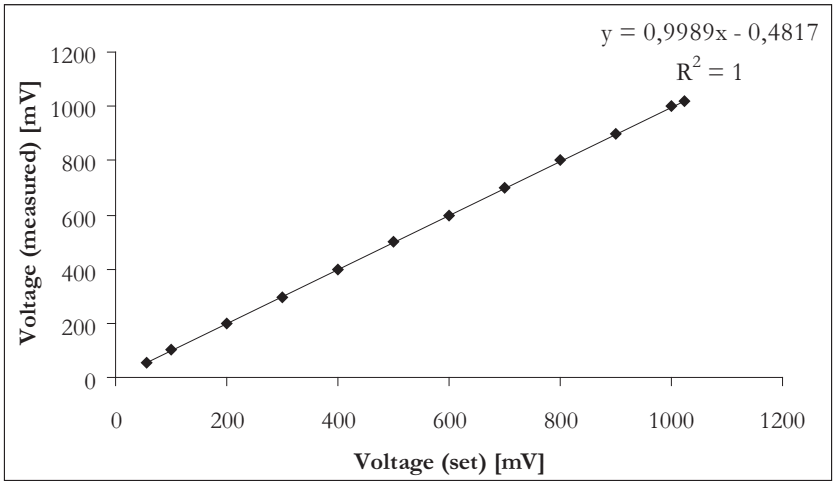

Figure 6.10: The voltage measured between the reference electrode (RE) and the substrate (WE) as a function of the voltage (set).

Reference samples were performed by withdrawing the substrate with the two rates chosen from previous experiments and from a 24 g/L suspension of PS particles i.e. no potential was applied to the substrates (as in Section 6.3.2, these Cr and Cu samples is used as one of the Cr refB and Cu refB samples in the duplicate of the present investigation in this section). Furthermore, samples applied a potential of 0 mV, 60 mV, and 300 mV were prepared. The samples and their designations can be seen in Table 6.6. The reference sample is not equal to the sample applied a potential of 0 mV. This is because the potential of the metal surfaces in a liquid is not known, when this is not controlled by the potentiostat. The PS suspension was prepared from batch 2.

Table 6.6: Samples prepared for the "Application of an Electric Potential" investigations. The rates are still named with B and C, as in the previous experiments (cf. Subsection 6.2.1). The suspension used was prepared from batch 2.

Substrate	Electric Potential [mV]	Rate B: $3{\cdot}10^{-2}$[mm/s]	Rate C: $1{\cdot}10^{-1}$[mm/s]
Cu	reference	Cu refB	Cu refC
Cu	0	Cu 0B	Cu 0C
Cu	60	Cu 60B	Cu 60C
Cu	300	Cu 300B	Cu 300C
Cr	reference	Cr refB	Cr refC
Cr	0	Cr 0B	Cr 0C
Cr	60	Cr 60B	Cr 60C
Cr	300	Cr 300B	Cr 300C

6.4.1 Stability of the Particle Zeta Potential

The stability of the zeta potential of the particles was tested. The samples, from Table 6.6, were prepared from the same suspension of PS particles. The samples were prepared in the order; Cu refB - Cu 300B, Cr refB - Cr 300B, Cu refC - Cu 300C, and Cr refC - Cr 300C. The zeta potential

of the PS suspension was measured in between the preparations of the different samples. The zeta potential of the particles was before this investigation measured to be 55 ± 2 (cf. Table 6.1). Because of problems with the PS particles contaminating the measure cell (in the Zetamaster S) the zeta potential after the preparation of Cr refB and Cr 60B are not present at the bar chart, that displays the results of the investigation, seen in Figure 6.11.

The zeta potential of the PS suspension was observed to be relatively stable throughout the preparations of the samples. All potentials lay around 50 mV. Only the zeta potential measured after the preparation of Cr 0C had a significant lower zeta potential. This lower potential seemed to be due to the problems with the apparatus during the measurements. The variations in the applied potential, and hereby the field applied to the suspension, did not have an influence on the particle zeta potential (Figure 6.11).

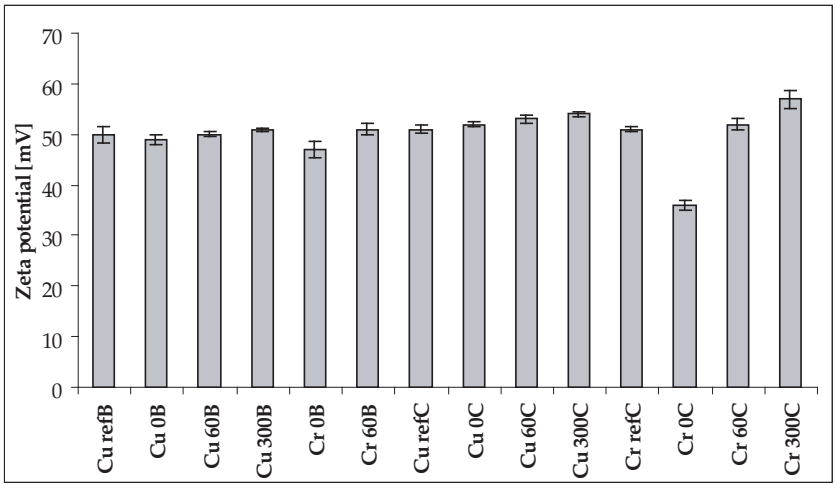

Figure 6.11: The zeta potential of the particles in the PS suspension during the investigation of application of potential. The samples were prepared in the order seen in the bar chart, starting with sample Cu refB and ending with Cr 300C. The column represents the zeta potential of the PS suspension measured after the preparation of the sample.

6.4.2 Application of an Electric Potential with Chrome as Substrate

From the measurements of current collected when applying an electric potential it was observed, that the Cr samples did not conduct electricity. The current measurements showed a constant value of zero, with minor deviations. This was the case when using both withdrawal rates, which can be seen in Figure 6.12 (a) and (b).

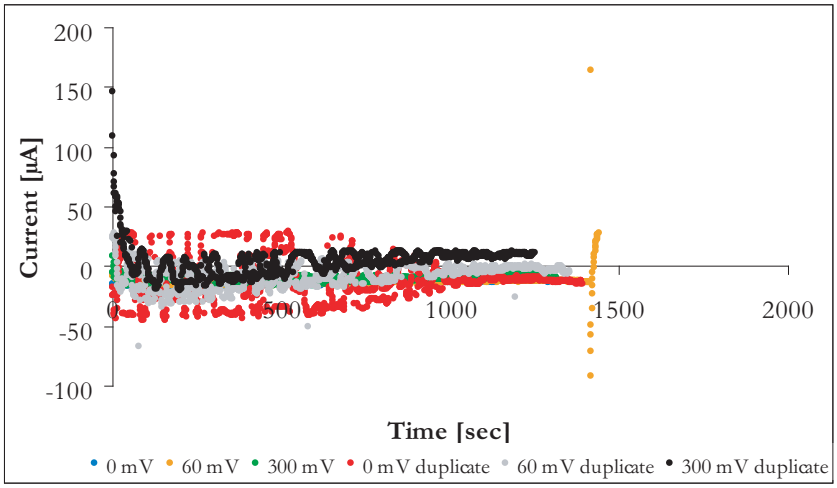

(a)

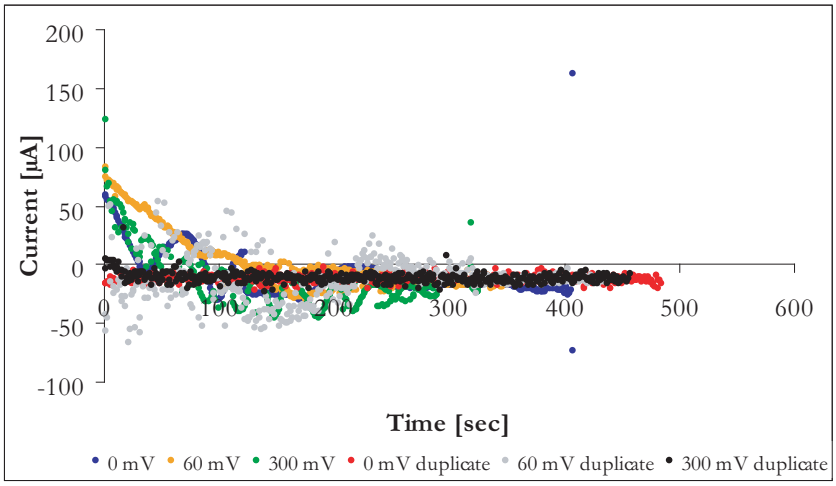

(b)

Figure 6.12: The current measurements during the preparation of the Cr samples with the potentials 0 mV, 60 mV, and 300 mV and the duplicate samples, with withdrawal rate (a): $3{\cdot}10^{-2}$ mm/s and (b): $1{\cdot}10^{-1}$ mm/s.

Furthermore, the SEM analysis showed no effect of the potential (the images can be seen on the enclosure CD - "Results" - "Potential experiments SEM"). Thus, the samples looked alike and were all comparable to the reference (cf. Figure 6.9). Because of the diverse depositions observed on the chrome surfaces, it was also difficult to see an effect of the faster withdrawal. However, the faster withdrawal seemed to contribute to less particles being deposited onto the surfaces, which was also expected from the results gained in Section 6.2. Besides, several of the curves in Figure 6.12 were observed to be oscillatory.

6.4.3 Application of an Electric Potential with Copper as Substrate

The potential was observed to contribute to a color change of the surface of the copper substrate i.e. from a normal "copper" color to a multicolored surface, as seen in Figure 6.13. This is expected to be due to oxidation of the surface, hence, the Cu substrates become coated with

verdigris. Furthermore, differences were observed between the four samples. It seemed like the film became thinner and more homogeneous with increasing potential. This indicates an effect of the applied potential is achieved. The distinct horizontal lines seen Cu 0B, Cu 60B, and Cu 300B is due to interruption of the film deposition.

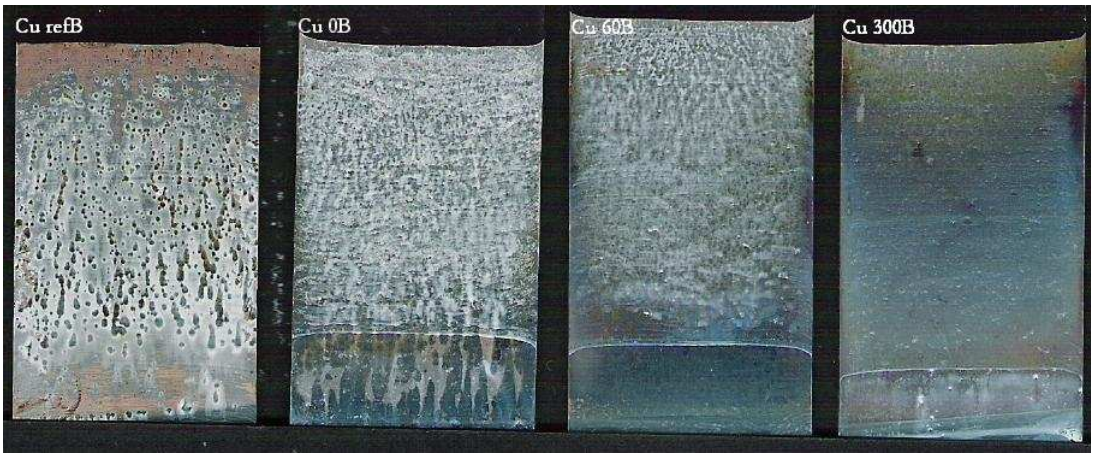

Figure 6.13: The samples of Cu withdrawn with $3{\cdot}10^{-2}$ mm/s and with varying electric potential of the Cu substrate. The electric potential of the substrate was varied from 0 - 300 mV.

The current measurement during the preparation of the Cu samples were observed to differ from each other in proportion to the current measurements of chrome, as seen in Figure 6.14. This must be due to the ability of Cu to conduct electricity.

The current measurement of the Cu samples prepared with rate : $3{\cdot}10^{-2}$mm/s, showed differences of the samples prepared with 60 mV and 300 mV, from the sample prepared with a 0 mV potential (see Figure 6.14 (a)). No current was present at 0 mV, and the current increased with increasing potential. Furthermore, the measurements were reproducible. Only minor deviations were seen between the curves of a sample and its duplicate. The curves of both the 60 mV samples and the 300 mV samples were with time moving toward a current of 0 μA. This is due to the area of the substrate (WE) immersed in the suspension becoming smaller because of the withdrawal. Thus, a current of 0 μA must indicate that a minor area or nothing of the substrate is immersed in the suspension (Figure 6.14 (a)).

The current measurement of the Cu samples prepared with rate : $1{\cdot}10^{-1}$ mm/s, showed like the last-mentioned measurements, differences of the samples prepared with 60 mV and 300 mV from the sample prepared with a 0 mV potential (see Figure 6.14 (b)). This time the differences between the three curves were more distinct. Again, no current was present at 0 mV, and the current increased with increasing potential. The measurements were reproducible. Again, the curves of both the 60 mV samples and the 300 mV samples were moving toward a current of 0 μA as a function of time. This time the decline was observed to be faster and with a larger slope, especially for the 300 mV samples. Again, this must be due to the area of the substrate (WE) immersed in the suspension becoming smaller because of the withdrawal. The earlier occurrence of the slope must be due to the faster withdrawal. Hence, the area of the substrate decreases faster. Moreover, a stagnation was observed in Figure 6.14 (b) for the 300 mV samples from around 0 sec and until around 150 sec. This is caused by the potentiostat not being able to contribute with the power needed. This could indicate, that the potentiostat was not able to

apply the desired 300 mV on the substrate. Again, Oscillating curves were observed, only the curves of the samples applied 300 mV had no distinct oscillating features (Figure 6.14).

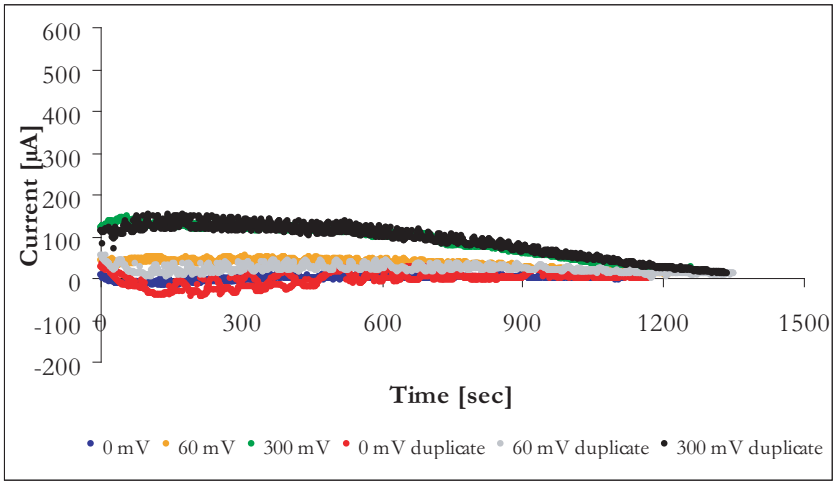

(a)

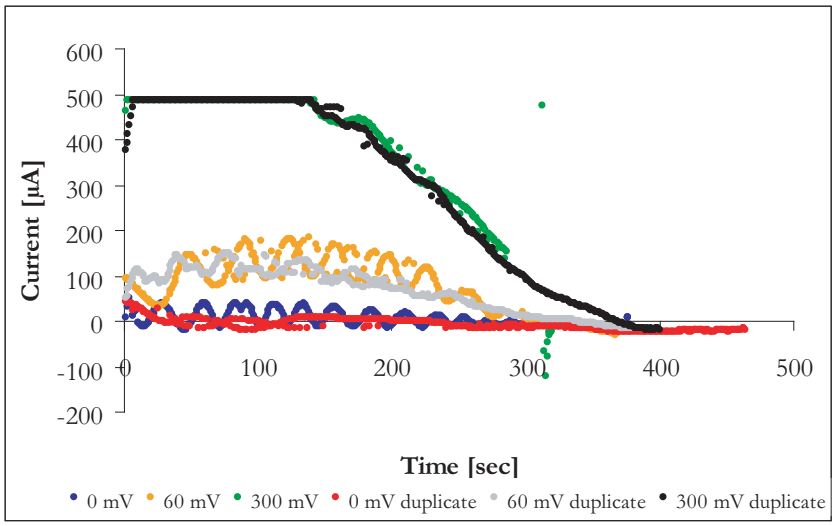

(b)

Figure 6.14: The current measurements during the preparation of the Cu samples with the potentials 0 mV, 60 mV, and 300 mV and the duplicate samples, with withdrawal rate (a): $3{\cdot}10^{-2}$ mm/s and (b): $1{\cdot}10^{-1}$ mm/s.

Additionally to the effect of the potential, seen in the current measurement and on the surface on the macroscopic level, the SEM analysis showed an effect of the applied potential.

The SEM analysis of the samples withdrawn with the rate of $3{\cdot}10^{-2}$ mm/s, seen in Figure 6.15, showed that the reference sample had large cracks in the film, which could indicate that large multi-layers were formed and hereby many particles were deposited on the Cu substrate (Figure 6.15, Cu refB). The sample applied a potential of 0 mV resembled the reference sample (Figure 6.15, Cu 0B). When applying a potential of 60 mV to the substrate, less cracks were observed, which could be caused by less particles being deposited on the surface (Figure 6.15, Cu 60B). Furthermore, a thinner film on sample Cu 60B observed in Figure 6.13, in proportion to Cu 0B,

also indicates that the potential is pushing particles away. With a potential of 300 mV the effect of the potential starts to be more marked. The substrate on the sample is now visible several places, which is due to the particles being repelled because of the positive substrate potential. In general, less particles were observed at the sample applied an electric potential of 300 mV (Figure 6.15, Cu 300B).

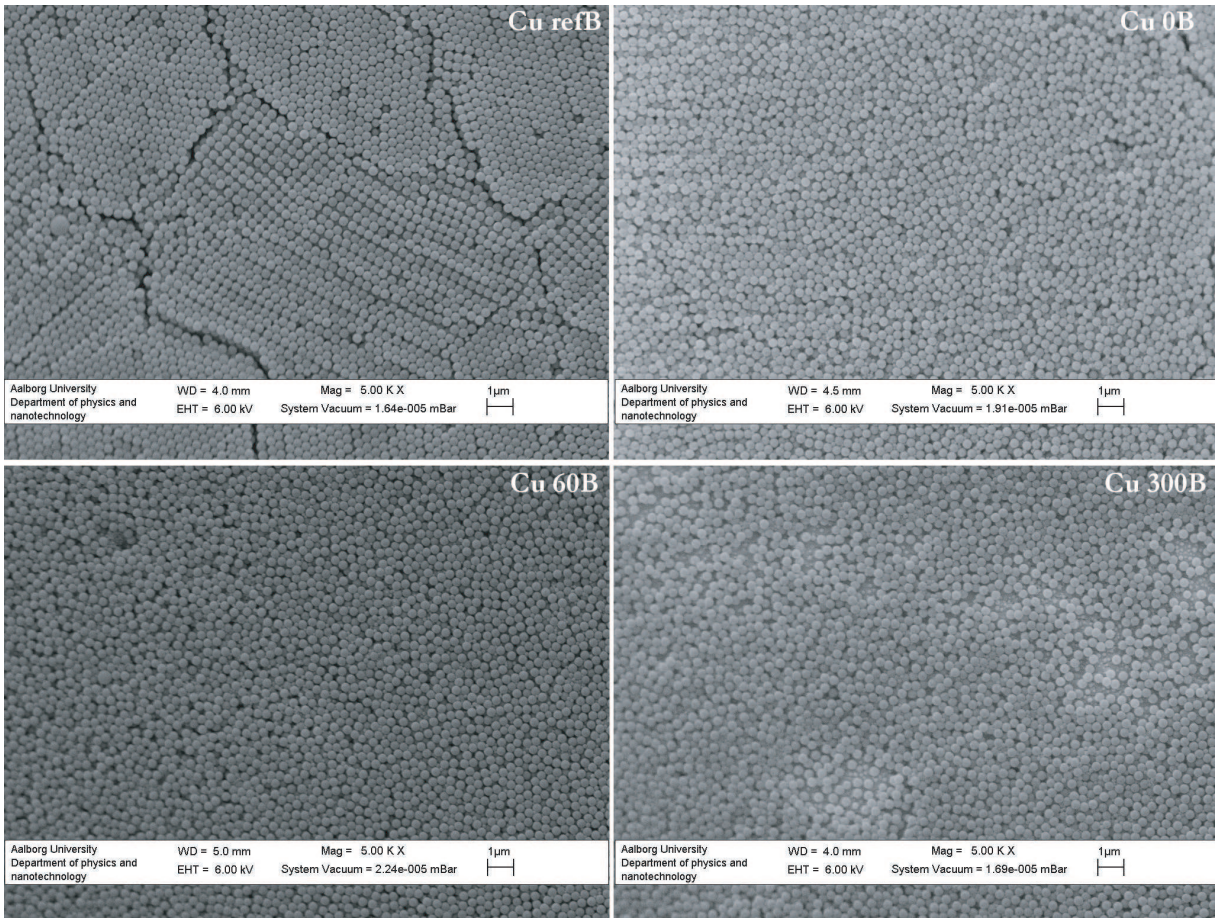

Figure 6.15: SEM images from the analyses of Cu refB, Cu 0B, Cu 60B, and Cu 300B. The samples were heterogeneous, therefore, the images shown are believed to represent the sample the best. The rest of the images can be seen on the Enclosure CD - "Results" - "Application of Potential" - "Potential Experiments SEM".

When withdrawing the samples with the rate of $1{\cdot}10^{-1}$ mm/s, generally less particles were observed to be deposited on the substrate, which was also expected from the higher withdrawal rate (see Figure 6.16). From the analysis of the reference sample, Cu refC, it was observed that the particles was now packing like it was observed at the Cr reference sample. The sample contained mono-layers where the particles were relatively CP with the desired hexagonal lattice, but still large areas where no packing occured were observed (Figure 6.16, Cu refC). The same observations, as the for the reference sample, is observed for the sample applied 0mV. Slight more particles seemed to be present at Cu 0C, though (Figure 6.16, Cu 0C). The sample applied a potential of 60 mV resembled the 0 mV sample (Figure 6.16, Cu 60C). Again, when applying a 300 mV potential, less particles were deposited on the surface. Primary mono-layers are observed which are relatively packed (Figure 6.16, Cu 300C).

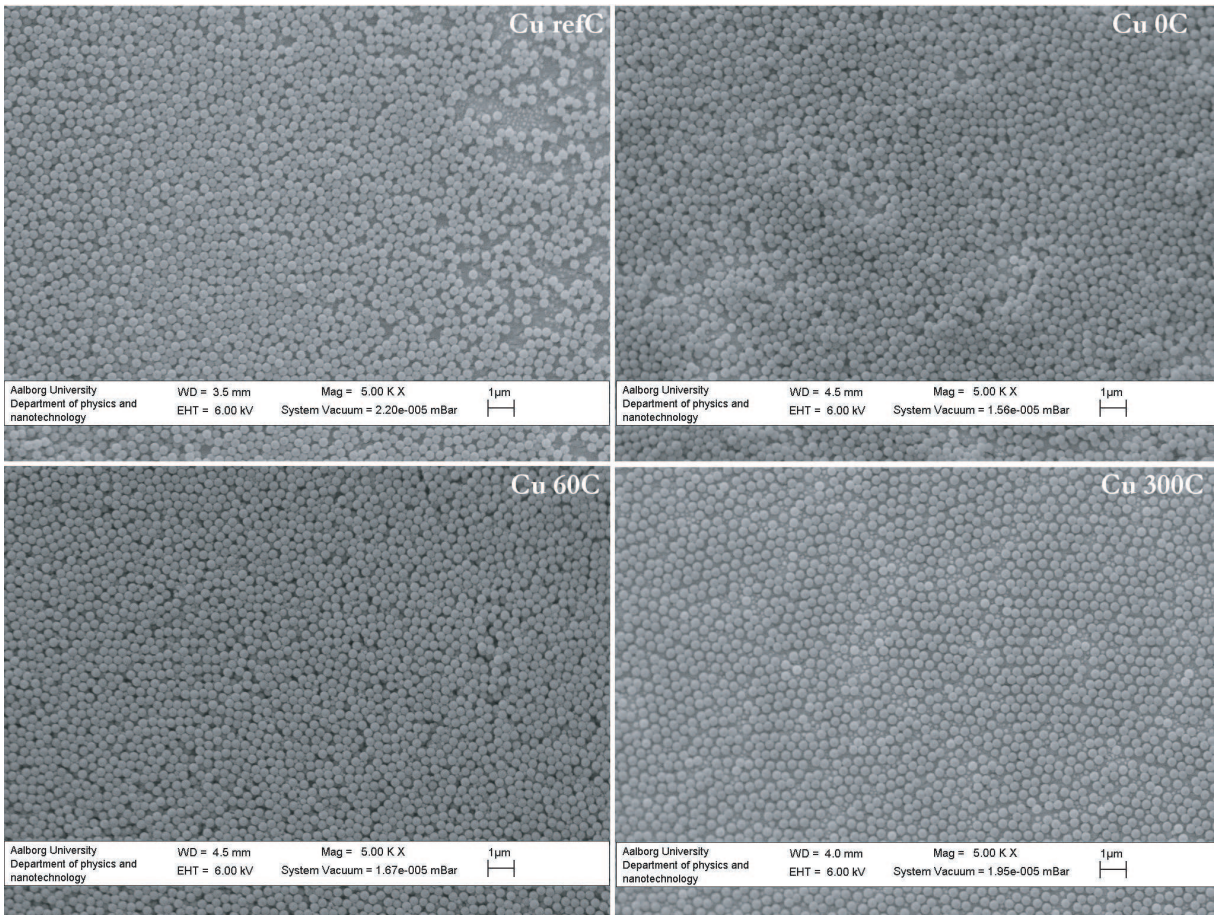

Figure 6.16: SEM images from the analyses of Cu refC, Cu 0C, Cu 60C, and Cu 300C. The samples were heterogeneous, therefore, the images shown are believed to represent the sample the best. The rest of the images can be seen on the Enclosure CD - "Results" - "Application of Potential" - "Potential Experiments SEM".

The reproducibility of the Cu samples observed from the current measurements were also observed in both macroscopic level (visually) and microscopic level (SEM). The samples were performed in duplicate, and in the macroscopic level the duplicates of the Cu surfaces at both rates were very identical. The computer scan of the samples withdrawn with $1{\cdot}10^{-1}$ mm/s and their duplicates are shown in Figure 6.17. It should be noted that the horizontal lines seen near the bottom of the substrates applied a potential, is caused by interruption of the film deposition. The other scans can be seen on the Enclosure CD - "Results" - "Application of Potential". On both Cu refC and Cu refC duplicate a relatively uniform film is deposited. Both the Cu 0C samples showed a film, which indicated that more particles were deposited, than on the reference. Thus, the film had a more pronounced white color. The samples added potentials of 60 mV and 300 mV seemed all to be oxidized, and the oxidation was most pronounced for samples applied a potential of 300 mV. Furthermore, the samples applied 300 mV potential seemed to have a thinner particle film, and the verdigris was significant on these samples.

In section 6.3.2, it was observed that the film deposited on the metal substrates were generally not as uniform as on the glass slides. From the SEM analysis of the Cu samples, it was observed, that when looking at the samples as a whole, the samples can be reproduced. The overall tendencies

Figure 6.17: Computer scans of the samples Cu refC, Cu 0C, Cu 60C, and Cu 300C and their duplicates.

in the samples were rediscovered (Enclosure CD - "Results" - "Application of Potential"). Both in macroscopic and microscopic level, the samples were relatively reproducible.

6.5 Removal of Particles from the Gold Coated Surface

Different methods of removing particles from gold coated surfaces were investigated. No surfaces with CP mono-layer of particles with a hexagonal lattice were obtained, therefore, these investigation were performed on the Cr samples from the experiments in Subsection 6.4.2. These samples were chosen, because all of the samples were generally similar, because no potential had been applied. Furthermore, mostly mono-layers and double-layers were observed. Hence, the investigations can be related to if the CP mono-layer of particles with a hexagonal lattice were obtained, and the particles were to be removed. The Cr samples had been coated with 20-30 nm Au before the SEM analysis.

From the investigations of heating the sample to 550° for 2 hours, the samples had obtained a more intense dark gold like color, than the gold color that had been observed straight after the coating of the sample. The images from the SEM analysis, see Figure 6.18 showed spherical material, which could be the PS particles. Yet, the size of the particles were smaller than the

initial size. Thus, degradation of the particles may have taken place, but not enough to remove the particles completely. Furthermore, large crystals of several micrometers were found on the surface after heating, which was probably due to the annealing of the Cr substrate. The large crystals of several micrometers and the smaller spherical materials with sizes in the nanometer scale seen from Figure 6.18, results in a two-scale structure, that could be compared to the leaves of the lotus flower. Unfortunately, the deformation of the samples during heating made it impossible to measure a water CA of the surface.

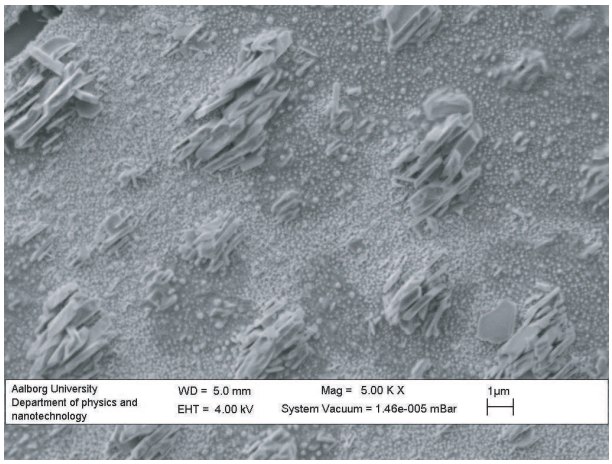

Figure 6.18: SEM image of the heat treated samples. The rest of the images can be seen on the Enclosure CD - "Results" - "Removal Test".

Moreover, it was from Figure 6.19 observed that these large crystals seemed to be relatively equally distributed all over the surface

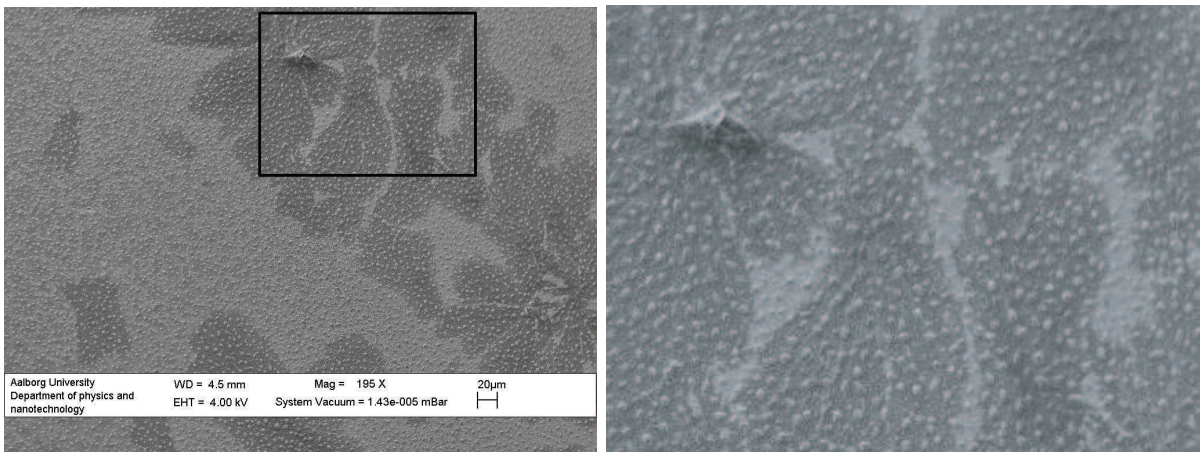

(a) (b)

Figure 6.19: SEM image of the heat treated surface, showing the microscale structure (a), and (b) an enlargement of the area marked in image (a). The rest of the images can be seen on the Enclosure CD - "Results" - "Removal Test".

The SEM analysis of the samples washed with toluene for 43 hours, see Figure 6.20, showed a lot of particles, thus, the washing method did not seem to have any significant effect of particle removal. Deformed particles were observed on the surface, though. Therefore, toluene had been

able to reach the particles, but not dissolve them totally.

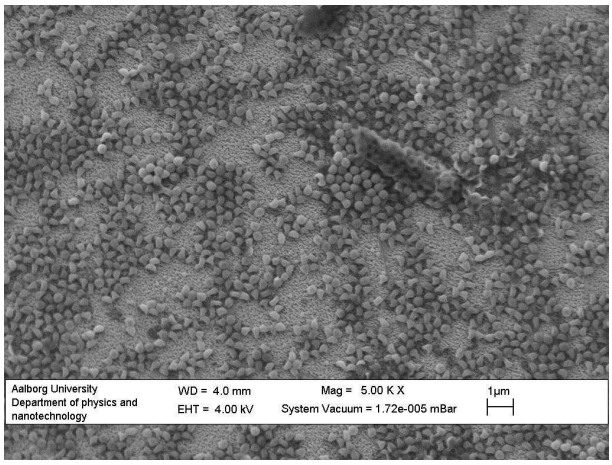

Figure 6.20: SEM image from a samples that have been washed in toluene for 43 hours. The rest of the images can be seen on the Enclosure CD - "Results" - "Removal Test".

The SEM images of the samples that had been sonicated in toluene for 5 minutes, see Figure 6.21, showed that the particles had been removed from the surface. Only few particles were observed on the surface during the analysis. It is from this experiment difficult to estimate, whether the gold coating, that has been deposited between the particles, were still present on the surface, or if the sonication had removed both particles and gold coating. This is mainly because of the thin layer of gold coated onto the surface. Moreover, the SEM images showed different shades of gray on the surface, which was not observed on the chrome surfaces from the other experiment.

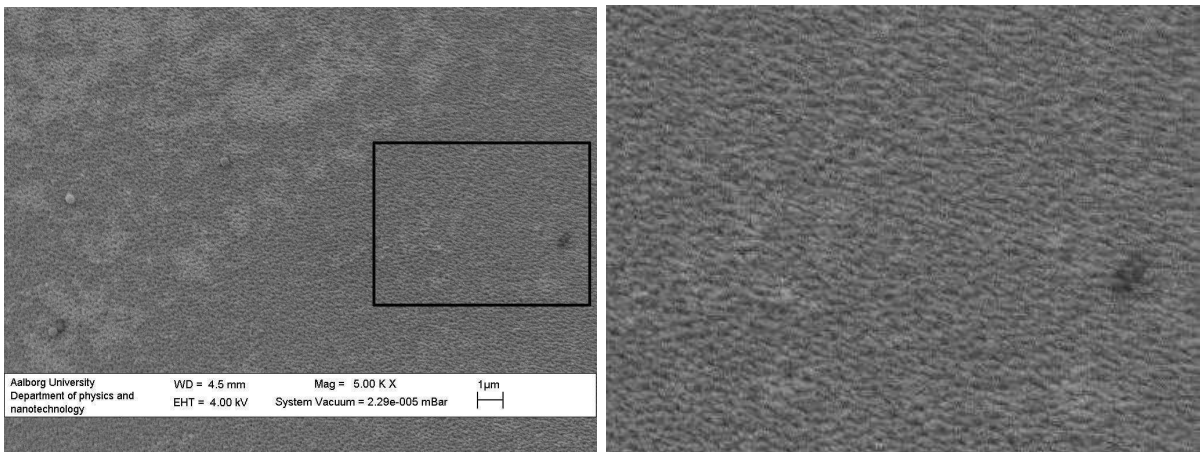

(a) (b)

Figure 6.21: SEM image from a sample sonicated for 5 minutes in toluene (a), and (b) an enlargement of the area marked in image (a). The rest of the images can be seen on the Enclosure CD - "Results" - "Removal Test".

Chapter 7

Discussion

The use of the thin liquid film techniques, the differences of the substrates, the application of an electric potential, and the removal of particles from a metal sputter coated surface, will be discussed on the basis of the results from the various analyses performed. Furthermore, the possibility of achieving a SH metal surface from the basic idea of the surface modification is discussed.

7.1 Particle Size

A model of the particle template system were prepared and it was from this concluded that the particle size did not have an influence on the CA obtained after modification. This was also confirmed from the work done by Abdelsalam and coworkers (2005). Nevertheless, it can be discussed whether there is an optimal particle size in connection to the technique used for the deposition of particles. Hanarp and coworkers (2003) found indications of stronger capillary forces with increasing particles size. Additionally, the brownian movements differs between different sized particles, hence, smaller particles moves faster than the larger particles. Whether the difference in kinetic energy of the different sized particles are able to influence the techniques is unknown.

7.2 Thin Liquid Film Deposition

From the investigation of "Withdrawal Rate and Polystyrene Concentration" (cf. Section 6.2) no CP particle mono-layer with a hexagonal lattice was achieved with the chosen rates and concentrations. Glass slides, which become negatively charged when immersed in water, and positively charged particles, were used for this investigation. This was according to Dimitrov and Nagayama (1996) a bad choice, because of large attractive coulomb forces hindering packing of the particles. Although, the mobility of the particles should be hindered by the attractive coulomb forces, the particles on samples with mono-layer seemed to assemble in smaller groups. The reason of the smaller groups could be because only the closest particles were able to attract one another enough to reach each other and assemble. It was also observed that sample B24 and

C24 formed larger groups of particles than the other samples and this could be due to a larger amount of particles present and hereby smaller interparticle distances and, therefore, attractions between the particles was observed. A high evaporation of water from the film on the prepared samples would also be an explanation of the lack of CP particle mono-layer with a hexagonal lattice. Because no humidity control is performed, the film dries to fast and hinders the mobility of the particles.

When using metal surfaces as substrate for the TLFD technique a different particle deposition was observed, than when using glass slides as substrates. More particles reached the surface. This could be due to the difference in surface energy, and hereby, the wettability. The glass surface was observed to be hydrophilic with a water CA of 20 $\pm$ 12°, and it is believed, that the particles possess a polar surface. This could be contributing to a hydration repulsion. Thus, water molecules will bound to the substrate and the particle surface, and hereby create a water shell around the surfaces. Moreover, both Cu and Al were observed to have a slightly hydrophobic surface, with water CA of 84 $\pm$ 7° and 85 $\pm$ 7°, respectively. In addition, chrome had a water CA of 95 $\pm$ 12° and was hydrophobic. Cu and Al seemed to have a relatively similar wettability. Still, large multi-layers were formed on the Cu substrates and mono- and double-layers on Al and Cr. It is difficult to involve the Al surface, because the particle deposition on this surface could mainly be due to the rough surface structure that hinders particle movement, and further acted like barbs when the Al substrate was withdrawn. But exactly the rough surface structure is a common feature of both Cr and Al. On Cr and Al less particles seemed to deposited, and the higher repulsion of these surfaces could be due to this structure. It was from the literature found that an increasing surface roughness contributed to increasing electrostatic forces [Suresh and Walz, 1996]. The van der Waals forces were also increased with increasing surface roughness, so whether the observation of less particle being deposited on the Al and Cr substrates, can be directed to the surface roughness is uncertain. However, the different depositions on the rough Al and Cr substrates in proportion to the smooth Cu substrates, in spite of the relatively similar water CA, indicates that surface roughness could play an important role. In addition, the multi-layers on the Cu substrates could be due to a slightly hydrophobic surface. When having a hydrophobic surface, hydrophobic attraction can occur. The PS particles possess a polar surface, but do still contain a hydrophobic core. Therefore, it is likely that a hydrophobic attraction could be present.

It was observed that the particles on the Cr refB and Cu refC had areas of CP particles in mono-layer with a hexagonal lattice. Hence, the particles seemed to have better possibilities of packing. This could be due to the surface possessing a positively charged surface, when immersed in water, which in accordance with Dimitrov and Nagayama (1996) would give the particles mobility and hereby larger possibilities of assembling. Many surfaces immersed in water possesses a negatively surface charge, though. Again, the enhanced mobility could also be due to wettability differences between the metal surfaces and the glass slides.

Whether wettability could be an explanation of, why the mono-layer/multi-layer shifts observed as horizontal lines on the glass substrates, was not observed on the metal substrates, is unknown.

7.3 Application of an Electric Potential

Cr was observed not to conduct the electricity applied in the investigations. This could be because Cr is oxidizing and a chromium oxide layer is formed on the surface. This layer seemed to stick to the surface and hereby functioned as an insulator. Therefore, it could have been investigated if larger voltages could have been conducted by Cr, and then an eventually effect of the potential could have been investigated. If larger voltages is applied, and these voltages exceeds 500 mV, particles will start migrating. In the system used in this work, the substrates were applied a positive potential to repel surplus particles. When the substrate is positively charged, the particles are positively charged, and the potential of the substrate is high to achieve an effect, there is a risk of too many particles migrating away from the surface. Only mono-layers and double-layers was observed on the Cr reference sample, so if too much particles migrates away from the surface, maybe, not enough particles will reach the surface to create a mono-layer.

From the current measurement when preparing the Cu samples, it was observed that different magnitudes of current was conducted. Of course, when shifting from 60 mV to 300 mV an increasing magnitude of conducted current would be expected. Still, larger magnitudes of conducted current was seen for a withdrawal rate of $1{\cdot}10^{-1}$ mm/s than when withdrawing the substrates with $3{\cdot}10^{-2}$ mm/s. From the SEM analysis of the samples it was observed, that less particles was deposited with a higher withdrawal rate. Therefore, the higher withdrawal rate, the larger magnitude of conductivity. This indicates, that when particles are present at the substrate the conductivity and hereby the resistance of the substrate is changed. The less particles, the higher conductivity.

An effect of the applied potential was observed as particles being repelled from the substrate. From the literature it was predicted that an electric field could enhance the lateral capillary force. Areas of CP particle mono-layer with a hexagonal lattice occurred when the metal surfaces were used, also without potentials, so an enhancement of the lateral capillary forces could not be concluded on the basis of these investigations. Maybe, if the field strength is increased, an enhancement of the capillary forces would be observed, as a larger attraction between the particles, and hereby close-packing of the particles. The effect was also by Trau and coworkers (1996) observed, to be large at higher voltages.

It could be investigated whether the conductivity of the sample can be a measure of when the formation of mono-layer is achieved. It would be a possibility of avoiding other more time-consuming analyses. Another property, that could be an indicator of when a CP particle mono-layer with a hexagonal lattice was achieved, is opalescence. Opalescence should be due to a systematic packing of particles, but still opalescence was observed on many of the samples in this work. This was especially on sample A24 in the investigation "Withdrawal Rate and Polystyrene Concentration" (cf. Section 6.2). The particles were systematically packed in large areas of the substrate, but multi-layer of particles were present. Therefore, one should be careful using this as an indicator of CP particle mono-layer with a hexagonal lattice. Additionally, more or less opalescence was observed on all samples in the investigation "Withdrawal Rate and Polystyrene Concentration" even though no packing was achieved. The slight opalescence on many of the samples could be due to that the samples contained mono-layers, where the particles were relatively equally distributed. Whether this relatively systematic packing can contribute to

the opalescence is unclear. But if this was the case, maybe, the magnitude of the opalescence could be an indicator of when a CP mono-layer of particles with a hexagonal lattice is achieved.

It was observed, that areas of CP mono-layer of particles with a hexagonal lattice turned up, when withdrawing the Cu reference with a higher rate. This could indicate the desired possibility of enhancing the withdrawal rate, and make the process faster. More investigations could be done on the application of potential to see, whether a optimal potential could be found that would form particle mono-layer with the concerned withdrawal rate. Furthermore, it could be interesting to investigate if a negative potential and an even faster withdrawal could create the CP mono-layer of particles with a hexagonal lattice. A faster withdrawal would in this case be necessary because of the coloumb forces that would be present, when having opposite charged surfaces. Dimitrov and Nagayama (1996) determined surfaces of same charge to be an criteria if a CP mono-layer of particles should be achieved. In proportion, it was from the investigations of Trau and coworkers (1996) observed that the application of an electric field was able to enhance the lateral capillary forces. Therefore, the opposite charges of the surfaces may not be important when combining the TLFD technique with an electric potential. Still, the opportunity of particle assemble could be hindered by this faster withdrawal, because of faster water evaporation from the film.

Oscillatory curves were observed from the current measurements. Direct current was used, so this can not be the reason. The potentiostat functions as a feedback system, why it could be possible, that the regulation of the surface potential of the electrode could cause the oscillations. The oscillating curves were observed for almost all current measurement from the sample preparation of Cu. But for the sample applied a potential of 300 mV at a rate of $1x10^{-1}$ mm/s, no oscillations were observed. The stagnation of the curve was determined to be caused by the potentiostat not being able to contribute with the power needed, and therefore, it could be possible that the feedback system keep the current flow at the highest level. This is not enough to reach the desired potential, and no oscillating curves are seen because of regulation. Another possibility could be that the observed oscillations were due to noise.

7.4 Removal of Particles from the Gold Coated Surface

From the investigation "Removal of Particles from the gold coated Surface" it was observed that only the method of sonicating the sample in toluene was able to remove the particles from the surface. Whether or not the gold was still present on the surface could not be concluded from the investigations. The samples were removed from the toluene and placed in a fume hood without further treatment. Therefore, the dissolved PS was present in the liquid, and may therefore have been deposited as a lipid layer on the surface, when drying the sample. The different gray colors observed on the surface could be due to this lipid layer. It could be an idea to rinse the surface with pure toluene, and maybe also water, after the removal of the sample from the sonication bath, and before the drying of the sample. The method, where the samples was left in toluene for 43 hours, showed particles that were partially dissolved. Maybe, if the duration was prolonged, the particles would have been dissolved. Furthermore, it could be a possibility to test the same method with another chemical. This should of course be a chemical, that generally, was observed to be able to dissolve PS particles. It can further be discussed whether changes in the stirring

rate would be able to alter the solvation of the particles. The heat treated samples showed large crystals on the surface. These crystals could be due to an oxidation of the surface forming chromium oxides. The crystals were observed to form islands on the surface. This could be due to the chromium oxide crystal minimizing there surface energy. Whether these large crystals could have been avoided, by lowering the heating temperature or a shorter duration, is unknown. From the investigation it seemed like the particles were still present at the surface, but had only shrunk. The temperature of 550°C for 2 hours should have removed all organic materials on the surface. Maybe, the gold layer hindered the decomposition of the particles. Still, the spherical material were observed all over the substrate surface, and they were observed to be of different sizes. Therefore, it is difficult to decide if it is PS or not. If the spherical material is the PS particles, lowering of the heating temperature or shortening the duration will not improve the removal of particles.

7.5 Superhydrophobic Metal Surfaces

From the modeling of the particle system a estimation of the water CA, that could be achieved with the different metals, was performed. According to the model a water CA of 153.2°- 156.7° can be obtained, with the metal candidates in this work. A SH surface posses a water CA higher than 150°. Therefore, it would be desirable if a higher CA, than the estimated, could be achieved. The wettability, and hereby the surface energy of the material that is modified, plays an important role. More specific, the surface energy of the material that the water drop is in contact with, plays an important role. The material that should be sputter coated onto the surfaces should possess a high water CA. Thus, the higher water CA the metal that is used for sputter coating posses, the higher CA of the modified surface can be achieved. Hence, an investigation of different materials and their CA could give an alternative to the metal candidates in this work. Furthermore, the size of the pillars play an important role in the obtained water CA. The smaller the area fraction of solid in contact with the water droplet, the higher a CA can be achieved. When working with particle templates, as in the present work, a smaller area fraction could be obtained, if, as an example, soft particles were used and these could be pressed together. Hereby, creating a smaller separation between the particles which would provide smaller pillars after the sputter coating and removal of the particles. Abdelsalam and coworkers (2005) achieved a water CA of 131° for a structured gold surface, and plane gold surface do normally posses a CA of 70°. From the modification in this work, nanopillars were expected, instead of the network structure, observed in the work by Abdelsalam and coworkers (2005). A larger solid fraction is expected from the network structure, than from an nanopillar structure. Therefore, it is probable that a successful modification with the technique and the metals in this work, could have given CA in the range estimated from the model. But, more work have to be done on the technique.

7.6 In a Larger Scale

The preparation of a particle template was investigated partially because the particle self-assemble was believed to function on a larger scale, in proportion to many other surface modification methods. If using the technique from the present work, the probability of using this on a larger scale can be discussed. The deposition on glass slides and pre-coated glass slide were investigated. Whether it would produce problems when depositing onto something larger than that, is not known. Furthermore, the withdrawal part of the method could create some problems if a particle film was to be deposited on curved surfaces.

Chapter 8

Conclusion

From the investigations it was found that a higher withdrawal rate contributed to less particles being deposited on the surface. Furthermore, more particles were deposited on the substrates with increasing polystyrene (PS) concentrations.

It was found, that the thin liquid film deposition (TLFD) technique was influenced by the wettability of the substrate and the surface of the particles that was to be deposited onto the substrate. Hydration repulsion seemed to be observed from the deposition of particles (with polar surfaces) on the hydrophilic glass substrate. A hydrophobic interaction seemed to take place between the hydrophobic substrate and the hydrophobic core of the particles. Furthermore, the differences of a planar and a rough surface structure seemed to give rise to an increased repulsion, which was observed by less particles being deposited on the rough surfaces in proportion to the planar surfaces.

Because of the formation of double- and multi-layers on the metal surfaces, when no potential was applied, it was decided to apply a positive potential to the substrates. The application of the electric potential was found to be able to control the particle deposition in the TLFD technique, by controlling the amount of particles deposited on the Cu surfaces. When applying a positive potential, less particles were deposited. No enhancement of the lateral capillary forces caused by the electric potential could be stated from this work.

No surfaces covered totally with CP particles in mono-layer with a hexagonal lattice were obtained from neither the TLFD alone, nor from the combination of the TLFD and an electric potential. Areas of CP particle mono-layer with a hexagonal lattice were observed at both Cu and Cr surfaces, but the film on the metal surfaces were also found to be heterogeneous.

Three different methods of removing particles from the sputter coated surface were investigated. Only the method of sonicating the sample in toluene for 5 minutes had removed the particles. Further investigation of the removal, including variation of the coating height of gold, must be performed to determine whether the particles can be removed and if the gold is still present at the surface. From this, it should also be possible to decide whether it is possible to obtain a rough structure on metal surfaces using a PS template.

Chapter 9

Future Work

It was from the investigations "Application of an Electric Potential" (cf. Section 6.4) observed that the potentiostat was, in case of sample Cu 300C, unable to contribute with enough efficiency to reach the desired potential. Therefore, a potentiostat with larger efficiency could be used in further investigations of the application of an electric potential to the substrates.

An investigation of the application of a potential of opposite charge than the particles could be performed. Then, when having opposite charges of the surfaces, it could be tested whether it was possible to apply a high potential (>500mV) and have a higher rate of withdrawal. The effect of the potential on the lateral capillary was not observed from the present work, but it is believed that a higher potential could be able to enhance these forces. This could be a possibility of making the process of film deposition faster, and of achieving the CP particle mono-layer with a hexagonal lattice.

Only few tests were performed on the removal of particles from a gold coated surface. The removal of the particles after the assembly and sputter coating is of significant importance to idea of modifying the surface with the particle template. Therefore, the methods including toluene could be performed with other organic solvents. These properties of the solvent could before the start of using be investigated, regarding to the their efficiency of solvating PS particles. Moreover, further investigations can be performed on the sonication method. Tests can be performed, where different amount of gold is sputter coated onto the surface, and the particles is attempted to be removed. From an experiment like this, it could possibly also be concluded whether the gold is still present at the surface or not.

Bibliography

[Abdelsalam *et al.*, 2005] M. E. Abdelsalam , P. N. Bartlett , T. Kelf, and J. Baumberg. Wetting of Regularly Structured Gold Surfaces. *Langmuir*, 21:1753–1757, 2005.

[Baumann *et al.*, 2003] M. Baumann , G. Sakoske , L. Poth, and G. Tünker. Learning from the Lotus Flower - Selfcleaning Coatings on Glass, 2003.

[Brett and Brett, 2000] C. M. A. Brett and A. M. O. Brett. *Electrochemistry; Principles, Methods, and Applications*. Oxford University Press, New York, 2000.

[Dimitrov and Nagayama, 1996] A. S. Dimitrov and K. Nagayama. Continuous Convective Assembling of Fine Particles into Two-Dimensional Arrays on Solid Surfaces. *Langmuir*, 12:1303–1311, 1996.

[DSA, 1980] DSA. Determination of Total Residue and Total Fixed Residue in Water, Sludge and Sediment. *Danish Standards Association*, 1:DS 204, 1980. In Danish.

[Eastman, 2005] J. Eastman. *Colloid Stability*. In Book: Colloid Science; Principles, Methods, and Applications, Editor: T. Cosgrove, Blackwell Publishing Ltd, 2005.

[Gilbert, 1995] R. G. Gilbert. *Emulsion Polymerization - A Mechanistic Approach*. Academic Press, 1995.

[Goodwin *et al.*, 2005] J.W. Goodwin , J. Hearn , C.C. Ho, and R.H. Ottewill. Studies on the Preparation and Characterization of Monodisperse Polystyrene Latices. *Colloid & Polymer Science*, 68:2495–2532, 2005.

[Goodwin, 2004] J. Goodwin. *Colloids and Interfaces with Surfactants and Polymers - An Introduction*. John Wiley & and Sons, 2004.

[Guo *et al.*, 2004] C. Guo , L. Feng , J. Zhai , G. Wang , Y. Song , L. Jiang, and D. Zhu. Large-Area Fabrication of a Nanostructure-Induced Hydrophobic Surface from a Hydrophillic Polymer. *ChemPhysChem*, 5:750–753, 2004.

[Hamley, 2006] I. W. Hamley. *Introduction to Soft Matter; Polymers, Colloids, Amphiphiles and Liquid Crystals*. John Wiley & and Sons, New York, 2006.

[Hanarp *et al.*, 2003] P. Hanarp , D. S. Sutherland , J. Gold, and B. Kasemo. Control of Nanoparticle Film Structure for Colloidal Lithography. *Colloids and Surfaces*, 214:23–36, 2003.

[Harris, 2002] D. C. Harris. *Quantitative Chemical Analysis*. W. H. Freeman and Company, New York, 6th edition, 2002.

[Hlavac and Rouer, 1997] F. Hlavac and E. Rouer. Expression of the Protein-Tyrosine Kinase $p56^{lck}$ by the ptrx Vector Yields a Highly Soluble Protein Recovered by Mild Sonication. *Protein Expression and Purification*, 11:227–232, 1997.

[Israelachvili, 1995] J. Israelachvili. *Intermolecular & Surface Forces*. Academic Press, 2nd edition, 1995.

[Jiang *et al.*, 2004] L. Jiang , Y. Zhao, and J. Zhai. A Lotus-Leaf-like Superhydrophobic Surface: A Porous Microsphere/Nanofiber Composite Film Prepared by Electrohydrodynamics. *Angewandte Chemie Int. Ed.*, 43:4338–4341, 2004.

[Kralchevsky and Nagayama, 2000] P. A. Kralchevsky and K. Nagayama. Capillary Interactions between Particles Bound to Interfaces, Liquid Films and Biomembranes. *Advances in Colloid and Interface Science*, 85:145–192, 2000.

[Li *et al.*, 2001] H. Li , X. Wang , Y. Song , Y. Liu , Q. Li , L. Jiang, and D. Zhu. Super-"Amphiphobic" Aligned Carbon Nanotube Films. *Angewandte Chemie Int. Ed.*, 40:1743–1746, 2001.

[Li *et al.*, 2007] X.M. Li , D. Reinhoudt, and M. Crego-Calama. What Do We Need for a Super-Hydrophobic Surface? A Rewiew on the Recent Progress in the Preparation of Super-Hydrophobic Surfaces. *Chemical Society Rewiews*, 36:1350–1368, 2007.

[Ma and Hill, 2006] M. Ma and R. M. Hill. Superhydrophobic Surfaces. *Current Opinion in Colloid & Interface Science*, 11:193–202, 2006.

[Martines *et al.*, 2005] E. Martines , K. Seunarine , H. Morgan , N. Gadegaard , C. D. W. Wilkinson, and M. O. Riehle. Superhydrophobicity and Superhydrophilicity of Regular Nanopatterns. *Nano Letters*, 5:2097–2103, 2005.

[Masliyah and Bhattacharjee, 2006] J. H. Masliyah and S. Bhattacharjee. *Electrokinetic and Colloid Transport Phenomena*. John Wiley & and Sons, New Jersey, 2006.

[Mate, 2008] C. M. Mate. *Tribology on the Small Scale; A Bottom Up Approach to Friction, Lubrication, and Wear*. Oxford University Press, New York, 2008.

[Min and Webb, 2001] J. Min and R. L. Webb. Condensate Formation and Drainage on Typical Fin Materials. *Experimental Thermal and Fluid Science*, 25:101–111, 2001.

[Mori, 2007] Y. Mori. Effect of Surface Hydrophobicity on Interaction between Particle and Flat Plate at Final Stage of Wet Coating Process. *Colloids and Surfaces A*, 311:61–66, 2007.

[Nagayama, 1996] K. Nagayama. Two-Dimensional Self-Assembly of Colloids in Thin Liquid Films. *Colloids and Surfaces*, 109:363–374, 1996.

[Pashley and Karaman, 2004] R. M. Pashley and M. E. Karaman. *Applied Colloid and Surface Chemistry.* John Wiley & and Sons, United Kingdom, 2004.

[Pozzato *et al.*, 2006] A. Pozzato , S.D. Zilio , G. Fois , D. Vendramin , G. Mistura , M. Belotti , Y. Chen, and M. Natali. Superhydrophobic Surfaces Fabricated by Nanoimprint Lithography. *Microelectronic Engineering*, 83:884–888, 2006.

[Qian and Shen, 2005] B. Qian and Z. Shen. Fabrication of Superhydrophobic Surfaces by Dislocation-Selective Chemical Etching on Aluminum, Copper, and Zinc Substrates. *Langmuir*, 21:9007–9009, 2005.

[Quere, 2005] D. Quere. Non-Sticking Drops. *Reports on Progress in Physics*, 68:2495–2532, 2005.

[Soanes and Stevenson, 2005] C. Soanes and A. Stevenson. *The Oxford Dictionary of English.* Oxford University Press, revised edition, 2005.

[Suresh and Walz, 1996] L. Suresh and J. Y. Walz. Effect of Surface Roughness on the Interaction Energy between a Colloidal Sphere and a Flat Plate. *Journal of Colloid and Interface Science*, 183:199–213, 1996.

[Trau *et al.*, 1996] M. Trau , D. A. Saville, and I. A. Aksay. Field-Induced Layering of Colloidal Crystals. *Science*, 272:706–709, 1996.

[Wang *et al.*, 1999] D.-Y. Wang , K.-W. Weng , C.-L. Chang, and W.-Y. Ho. Synthesis of Cr_3C_2 Coatings for Tribological Applications. *Surface and Coatings Technology*, 120-121:622–628, 1999.

[Wang *et al.*, 2008] X. Wang , J. A. Kluge , G. G. Leisk, and D. L. Kaplan. Sonication-Induced Gelation of Silk Fibroin for Cell Encapsulation. *Biomaterials*, 29:1054–1064, 2008.

[Yang *et al.*, 2006] C. Yang , U. Tartaglino, and B.N.J. Persson. Influence of Surface Roughness on Superhydrophobicity. *Physical Rewiew Letters*, 97:116103, 2006.

Appendix A

Surface Wettability

A direct expression of the wettability of a surface is given by Young's equation, which expresses the wettability by means of a CA of a water droplet on a flat surface (Equation A.1)[Li *et al.*, 2007].

$$cos\theta = \frac{\gamma_{SV} - \gamma_{SL}}{\gamma_{LV}} \tag{A.1}$$

γ_{SV}, γ_{SL}, and γ_{LV} refer to the interfacial surface tensions between solid(S), liquid(L), and vapour(V). Young's angle (θ) results from the thermodynamic equilibrium of the free energy at the solid-liquid-vapor interface. Young's angle determines whether the surface properties are hydrophobic ($\theta > 90°$) or hydrophilic ($\theta < 90°$). Low surface tension materials contributes to high CAs [Ma and Hill, 2006]. Two types of CA are used; static and dynamic CAs. The static CA is corresponding to Young's angle when having a flat surface. When measuring the static CA, a drop is placed on a surface and the value is obtained by a goniometer. The dynamic CAs are non-equilibrium CAs, which are measured during growth (advancing CA, θ_a) and shrinkage (receding CA, θ_r) of a water droplet. The difference between θ_a and θ_r is defined as the CA hysteresis ($\Delta\theta$). SH surfaces possess, as mentioned earlier, a water CA higher than 150°. This very high CA is normally called apparent CA because the value does not represent the "real" CA value corresponding to flat surfaces [Li *et al.*, 2007].

When having a rough surface, a water droplet can either penetrate the pillars or suspend above the pillars, as illustrated in Figure A.1.

Figure A.1: Illustration of the Wenzel model (left) and the Cassie-Baxter model (right)

In both cases much higher CAs are obtained, than when having a water droplet on a flat surface. The penetration of the water droplet is described by the Wenzel (W) model. When having a thermodynamic equilibrium, a linear relationship between the apparent CA and the roughness factor appear, given by Equation (A.2)[Li *et al.*, 2007].

$$cos\theta^W = rcos\theta \tag{A.2}$$

θ^W corresponds to the apparent CA (when having the W state), and θ represent the Young's angle. r represents the roughness factor and is defined by the actual surface area divided by the projected surface area. A rough surface thereby gives r $>$ 1. Wenzel's prediction for a hydrophobic surface gives $\theta^W > \theta > 90°$ and a hydrophilic surface gives $\theta^W < \theta < 90°$. The roughness of the surface enhances both hydrophobicity and hydrophilicity depending on the nature of the corresponding flat surface. For a hydrophobic surface the CA and its hysteresis increases as the roughness increases. A steadily increase of the CA with roughness is seen until r $>$ 1.7. Then the CA hysteresis decreases contrary to the Wenzel's prediction. This decrease in CA hysteresis is attributed to the switch from W state to the Cassie-Baxter (CB) state, which is caused by the increasing roughness contributing to increased air fraction. This leads to a suspension of the water droplet on top of the pillars (a composite state) which is described by the CB model. The switch from the W to the CB state entails that the apparent CA is now described as the sum of all the contributions of the different phases, given by Equation (A.3) [Li *et al.*, 2007].

$$cos\theta^C = f_1 cos\theta_1 + f_2 cos\theta_2 \tag{A.3}$$

θ^C is the apparent CA (when having the CB state), f_1 is the surface fraction of phase 1, which is the area in contact with liquid divided by the projected area, and f_2, surface fraction of phase 2, is the area in contact with air divided by the projected area. θ_1 and θ_2 is the CA of phase 1 and 2, respectively. When having only one type of pillars, and given that f is the solid fraction, then the air fraction can be described by (1 - f). With $\theta_2 = 180°$, the CA can be calculated from Equation (A.4) [Li *et al.*, 2007].

$$cos\theta^C = f(1 + cos\theta) - 1 \tag{A.4}$$

The apparent CA is, when using the CB model, a sole function of the solid fraction for a given θ. To obtain a SH surface, the contribution of the solid fraction must be as small as possible or/and the used material must posses as low a surface energy as possible. Both theories, Wenzel and CB, do only give a qualitatively information of the CA on a rough surface. Hence, the decision of which theory to use is difficult [Li *et al.*, 2007].

Appendix B

Modeling of the Particle System

This model is made to decide the particle size and the coating height that are optimal when modifying the metal surfaces. Furthermore, the model gives an estimation of the CA that can be obtained from the used method. This is of cause dependent on the water CA's of the metal surfaces. Cr, Al, and Cu with water CA's of 82 $\pm 5°$[Wang *et al.*, 1999], 81°, and 97° [Min and Webb, 2001], respectively, are the metal surfaces available.

It is desired to obtain particles self-assembled in a CP hexagonal pattern. This pattern can be described by the repeating unit given i Figure B.1). By the red triangle (the repeating unit) the solid fraction after coating, which is represented by the gray "triangle" between the particles, can be calculated as follows.

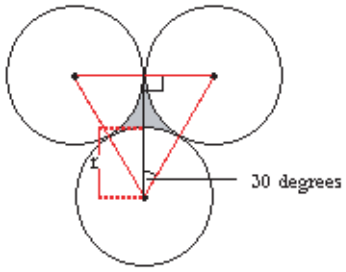

Figure B.1: An illustration of the repeating unit marked with a red triangle, which is expected in a CP hexagonal pattern. The grey area corresponds to the pillar that will be left after coating and removal of the particles.

The particles used to form the template are expected to be monodisperse. It is seen from the repeating unit, that 1/6 of each of the three particle cross-sectional areas ($A_{particle}$) contributes to the repeating unit. This corresponds to the cross-sectional area of half a particle, that is given by Equation (B.1).

$$A_{particle} = \frac{1}{2}\pi r_{particle}^2 \tag{B.1}$$

The area of the repeating unit $A_{repeating}$ (sketched in Figure B.1) is calculated from the cosine relation, as seen from Equation (B.2)-(B.3).

$$A = \frac{1}{2} \cdot height \cdot width \tag{B.2}$$

$$A = \frac{1}{2} \cdot Ccos(30) \cdot C \tag{B.3}$$

Where C is the center-to-center distance. In this case C equals two times the radius of a particle, and therefore $A_{repeating}$ is given by Equation (B.4).

$$A_{repeating} = 2 \cdot r^2_{particle} cos(30) \tag{B.4}$$

A_{pillar} is then given by Equation (B.5).

$$A_{pillar} = A_{repeating} - A_{particle} \tag{B.5}$$

that becomes:

$$A_{pillar} = 2 \cdot r^2_{particle} cos(30) - \frac{1}{2}\pi r^2_{particle} \tag{B.6}$$

The solid fraction is given by the area of the pillar divided by the total area (the area of the repeating unit)(Equation B.7).

$$f = \frac{A_{pillar}}{A_{repeating}} \tag{B.7}$$

When looking at the solid fraction as a function of particle size only it is given by Equation (B.8).

$$f_{particle\ size} = \frac{2r^2_{particle} cos(30) - \frac{1}{2}\pi r^2_{particle}}{2r^2_{particle} cos(30)} \tag{B.8}$$

When reducing Equation (B.8) it gives :

$$f_{particle\ size} = \frac{2cos(30) - \frac{1}{2}\pi}{2cos(30)} = \frac{cos(30) - \frac{1}{4}\pi}{cos(30)} \approx 0.093 \tag{B.9}$$

From Equation (B.8) it is found, that the particle size has no influence on the solid fraction, but gives a constant solid fraction of 0.093.

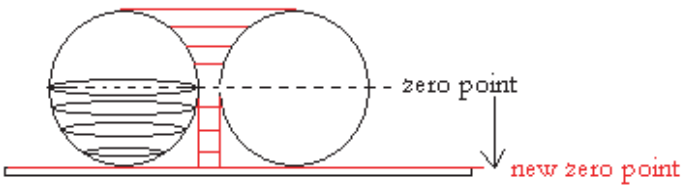

Figure B.2: An illustration of how the coating height influences the particle cross-sectional area, and hereby the area left after coating and removal of the particles.

From Figure B.2 it can be seen that the coating height will have an influence on the solid fraction. Furthermore, this was also observed in the work by Abdelsalam and coworker (2005) (cf. Chapter 2). This is caused by a varying in cross-sectional area of the particle as a function of coating height (still, half a particle area contributes to the repeating unit). The cross-sectional area as a function of coating height (n) is give by Equation (B.10).

$$A_{cross} = \frac{1}{2}\pi(r_{particle}^2 - (n - r_{particle})^2) \tag{B.10}$$

The solid fraction is then given by Equation (B.11):

$$f_{coating\ height} = \frac{A_{repeating} - A_{cross}}{A_{repeating}} \tag{B.11}$$

which results in Equation (B.12):

$$f_{coating\ height} = \frac{2r_{particle}^2 cos(30) - \frac{1}{2}\pi(r_{particle}^2 - (n - r_{particle})^2}{2r_{particle}^2 cos(30)} \tag{B.12}$$

The solid fraction as a function of coating height is entered into the Cassie-Baxter equation, and Equation (B.13) is obtained.

$$cos\theta^C = \left(1 - \frac{\pi(r_{particle}^2 - (n - r_{particle}))^2}{4r_{particle}^2 cos(30)}\right)(1 + cos(\theta)) - 1 \tag{B.13}$$

θ^C plotted as a function of coating height shows, that the optimal coating height is n = $r_{particle}$ and that according to the model a θ^C for Cr, Al, and Cu, of about 153.4°,153.2°, and 156.7° can be obtained, respectively (see Figure B.3).

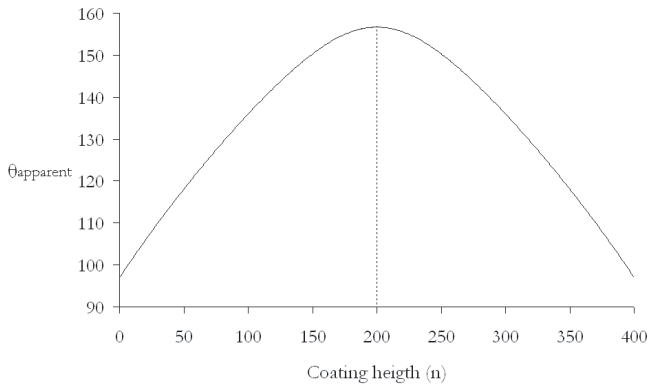

Figure B.3: The apparent water CA as a function of the coating height obtained using the Cassie-Baxter model. The data is calculated using copper as the material, $r_{particle}$ = 200 nm and n varying from 0 to $2r_{particle}$.

In the range from 1-199 nm, the model in Figure B.3 do not fit the system, because the model assumes that the variation in coating height is as seen in Figure B.4.

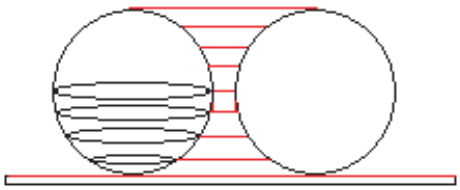

Figure B.4: An illustration of the coating height variations assumed by the model.

This is not expected to be the case in the system in the present work. An alternative could be assuming that the curve looks like in Figure B.5, because the pillars are expected to have the same cross-sectional area until after 200 nm.

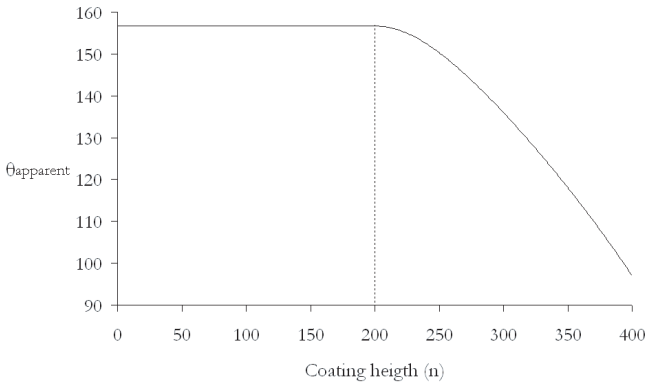

Figure B.5: The apparent water CA as a function of the coating height obtained using the Cassie-Baxter model. The data is calculated using copper as the material, $r_{particle}$ = 200 nm and n varying from 0 to $2r_{particle}$.

Still, the CA when having a coating height of 0 nm will not give rise to a contact angle of 156.7°, but instead the surface will possess a CA of a planar Cu surface. From this model the highest water CA possible, seems to be obtained when the coating height equals the radii of the particles. Coating heights in the range of 1-199 nm are not believed all to give rise to a contact angle of 156.7°, but whether some of them could, can not be concluded from this model.

Appendix C

The "Dipper" and the Set-up

The "Dipper" is an apparatus, specially constructed for this project, and was used when the studying the possibility of creating colloidal templates on various substrates. The "Dipper" was used to perform a TLFD technique and can withdraw substrates vertical, and with different rates.

Materials

- Motor : 23 frame size hybrid stepper motor, 200 steps/rev.
- Control PCB: 4 phase unipolar step motor drive board.
- 2×33 ohm, 25W power resistors and an aluminum cooling plate (with ribs) mounted with a 24 V fan as cooling system for the power resistors.
- Gearbox: 25:1.
- Power supply: Siemens SITOP, DIN-rail, PSU, 24V, 5A.

Furthermore, a slide holder was made. The apparatus can be seen in Figure C.1 in the set-up for the investigations of applying an electric potential.

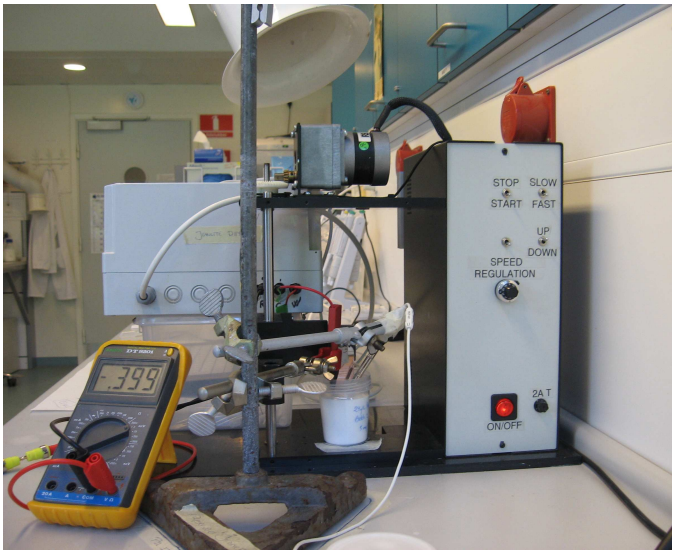

Figure C.1: The set-up for the investigations of applying an electric potential to the TLFD technique.

Enclosure I

Calibration of the Potentiostat

Calibration of the program and the potentiostat. The voltage and the current were calibrated by applying a voltage and measure the output voltage with a multimeter, the result is seen in Figure I.1(a), and applying a voltage and then read off the current at the display in the program (Enclosure CD - "Program") and at the display at the multimeter, result seen in Figure I.1 (b).

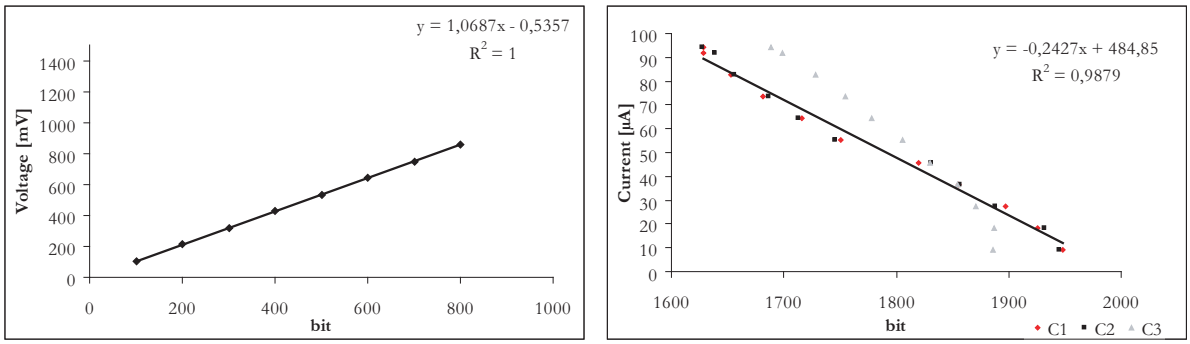

(a) (b)

Figure I.1: Calibration of (a) : the voltage and (b): the current. The C1-C3 are three different calibration series, where C1 and C2 were measured at the same time. The duplicate was made just after the first measurement. Calibration 3 was a data-set made separate from the other calibrations. The room temperature was 22°C while calibrating the current.

In Figure I.1 (b), calibration curve 3 (C3) was observed to differ from the other calibrations curves. This difference was observed to be due to heating up of the resistance and the capacitor during the three calibrations. Therefore, only C1 and C2 are concluded to be valid, because influence of the heat-up of the equipment is not as marked at these samples.